Applied Energy 416 (2026) 127957

Contents lists available at ScienceDirect

Applied Energy

journal homepage: www.elsevier.com/locate/apen

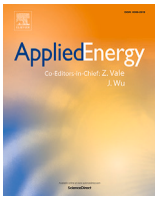

An incentivized automated market maker-based batch auction mechanism for network-aware local energy markets with loss allocation

Hossein Saber[1], Tom Celig[1], Saber Talari*, Wolfgang Ketter, Detlef Schoder

Cologne Institute for Information Systems (CIIS), University of Cologne, Cologne, North Rhine-Westphalia, Germany

HIGHLIGHTS

- Propose an automated market maker-based batch auction mechanism for illiquid, decentralized P2P local energy markets.
- Develop an on-chain modeling of distribution network constraints and fair loss allocation.
- Verify incentive compatibility of the proposed novel P2P energy trading mechanism.
- Implement a blockchain smart contract prototype enabling secure, transparent, and automated execution.
- Benchmark the proposed model against traditional double auctions and uniform-price auctions, demonstrating superior community self-consumption and overall welfare under real-world data simulations.

ARTICLE INFO

Keywords:
Energy communities
Liquidity provision
Local energy sharing
Smart contracts
On-chain power flow
Loss-allocation mechanism

ABSTRACT

The rapid proliferation of distributed energy resources demands efficient, fair, and scalable local energy markets (LEMs) that maximize community self-consumption while ensuring equitable trading outcomes. This paper introduces an incentive compatible Automated Market Maker-based Batch Auction (AMMBA), a novel peer-to-peer (P2P) market mechanism that leverages decentralized finance (DeFi) pricing principles to overcome liquidity scarcity, mitigate price volatility, and enable continuous market participation even in thin LEM environments. The pricing function parameters are optimized to balance consumer utility and supplier profit, while a penalty-driven mechanism guarantees dominant-strategy incentive compatibility, preventing misreporting and strategic withholding by market agents. To ensure technically valid operation, an integrated on-chain power flow formulation enforces distribution network constraints, including voltage and power flow limits, and automatically applies least-cost corrective demand or generation adjustments. Additionally, an ex-post loss allocation scheme, based on the concept of marginal loss factor, fairly assigns positive or negative power-loss impacts to participants, and trading payments are adjusted accordingly to maintain economic fairness. All trading, grid-feasibility assessment, loss allocation, and settlement processes are executed via blockchain smart contracts for full transparency and automation. The proposed AMMBA model is prototyped and evaluated using real-world household profiles and benchmarked against traditional double auction and uniform-price auction mechanisms. Results demonstrate that AMMBA significantly enhances community self-consumption, stabilizes clearing prices, increases social welfare and equality of benefit distribution, and reliably enforces grid operational constraints while ensuring fair loss allocation.

* Corresponding author.
Email addresses: saber@wiso.uni-koeln.de (H. Saber), celig@wim.uni-koeln.de (T. Celig), talari@wiso.uni-koeln.de (S. Talari), ketter@wiso.uni-koeln.de (W. Ketter), schoder@wim.uni-koeln.de (D. Schoder).

[1] These authors contributed equally to this work.

https://doi.org/10.1016/j.apenergy.2026.127957
Received 20 December 2025; Received in revised form 16 March 2026; Accepted 19 April 2026
Available online 30 April 2026
0306-2619/© 2026 The Authors. Published by Elsevier Ltd. This is an open access article under the CC BY license (http://creativecommons.org/licenses/by/4.0/).

1. Introduction

1.1. Background and motivation

The ongoing European Union (EU) green energy transition has accelerated the deployment of distributed energy resources (DERs), particularly renewable energy technologies such as photovoltaic (PV) and wind power. Consequently, investments in DERs are growing sharply across member states to meet decarbonization and energy independence targets [1]. This rapid proliferation of decentralized generation is transforming distribution networks from passive infrastructures into active systems with bidirectional power flows and complex operational dynamics. For instance, the global installed capacity of PV generation has surged from approximately 40 GW in 2010 to 2.2 TW in 2024 [2]. As a result, many traditional consumers are now becoming prosumers, who both produce and consume electricity [3].

The energy community concept, as formalized under the EU Directives 2018/2001 (Renewable Energy Directive II) and 2019/944 (Electricity Market Directive), plays a crucial role in aggregating distributed assets and prosumers to achieve operational scalability and enhance the efficiency of asset coordination [4]. By enabling collective ownership, governance, and participation, energy communities can facilitate the integration of renewable energy at the local level while promoting social acceptance and fairness in market participation [5,6].

Regulatory frameworks such as the feed-in tariff (FiT) scheme were introduced, offering guaranteed fixed payments for surplus renewable energy exported to the grid. However, FiT scheme often compensates prosumers at significantly lower rates than retail prices, limiting their economic attractiveness [7]. For example, in Germany, while the average residential electricity price in early 2024 was around 0.40 e/kWh [8], the FiT for solar PV energy was only 0.08 e/kWh [9]. To overcome such economic inefficiencies, local energy markets (LEMs) have emerged as a promising coordination framework for resource allocation with economic signals. Within LEMs, peer-to-peer (P2P) trading mechanisms allow prosumers to sell surplus energy directly to nearby consumers at prices negotiated between the FiT and retail levels, benefiting both parties: prosumers receive higher compensation, and consumers access cheaper local energy [10]. Among various market-clearing mechanisms, auction-based models—with frequent bid and offer updates—are particularly effective for establishing fair and dynamic local prices that reflect real-time supply and demand.

Nevertheless, even with community-based aggregation, auction-based local markets often suffer from limited liquidity, which may hinder efficient price formation and stable operation. This challenge highlights the need for robust market designs and automated clearing mechanisms capable of maintaining incentive compatibility, fairness, transparency, and scalability. In this regard, blockchain technology and smart contracts offer a viable solution. The decentralized and tamper-proof architecture of blockchain can ensure trust, transparency, and automation in local transactions, while Automated Market Maker (AMM)-based mechanisms can continuously provide liquidity without requiring a centralized market operator [11–13].

While financial settlements in these digital markets can be efficiently automated, it remains essential to ensure that physical energy delivery and grid constraints within the community network are respected. Thus, the on-chain grid-aware operational model is an important aspect of blockchain-based market mechanism design.

1.2. Related works

LEMs have historically employed conventional trading mechanisms such as order-book auctions and bilateral negotiation, but these approaches encounter fundamental challenges in nascent citizen energy communities. In particular, double auction (DA) mechanisms rely on a deep order book of bids and offers to discover prices efficiently. In the context of a small or emerging LEM, the market is inherently “thin”, leading to wide bid-ask spreads, volatile prices, and frequent trade failures [14–16]. A single large order can disproportionately sway the clearing price, undermining price stability and fairness in a low-liquidity setting [17,18]. Simplified single-sided auction models (in which only buyers or only sellers bid) have been tested to reduce complexity, but these tend to create power imbalances: the non-bidding side is forced to accept prices unilaterally, which can result in unfair outcomes that do not reflect real-time local supply–demand balance [18]. Fully decentralized negotiation-based schemes (e.g., bilateral bargaining or P2P matching) grant participants more autonomy, yet they suffer from high coordination overhead and poor scalability as participant numbers grow [19,20]. The iterative communication and computation required by negotiation models make them too slow and cumbersome for the fast, frequent transactions in a dynamic LEM [21]. These limitations highlight the need for alternative market designs that can ensure liquidity, price stability, and fairness without assuming a large pool of continuous bids.

To address issues of trust and coordination in LEMs, a growing body of work explores blockchain-based P2P trading platforms. The decentralized, tamper-proof architecture of distributed ledgers enables transparent and automated execution of local transactions, eliminating reliance on a centralized market operator. For example, Alskaif et al. [22] propose a fully decentralized residential P2P market that decomposes the centralized clearing optimization into a consensus-based algorithm, implemented via smart contracts for transparency and security. Abdella et al. [23] develop a blockchain platform to unify heterogeneous local markets, achieving higher throughput and lower latency for P2P trades compared to public blockchain frameworks. A game-theoretic double auction mechanism is presented in [24] to maximize social welfare while preserving prosumer privacy; the authors demonstrate that their blockchain implementation can ensure fair allocations and achieve incentive compatibility for participants. Similarly, Esmat et al. [25] introduce a two-layer market architecture where an off-chain heuristic auction optimizes allocations and an on-chain layer handles secure, real-time settlement of trades. These and other studies in the literature focus on enhancing transparency, automation, and decentralization in LEM operations. They show that blockchain smart contracts can facilitate reliable P2P energy exchanges with minimal human intervention and improved security. However, most such frameworks still adopt traditional auction-based clearing and thus inherit the aforementioned liquidity and volatility issues.

Drawing inspiration from decentralized finance (DeFi), AMM mechanisms have recently been proposed as an alternative market paradigm for P2P energy trading. AMMs replace the discrete matching of an order book with continuous liquidity pools and algorithmic pricing formulas, theoretically guaranteeing that a trade can clear at any time regardless of order book depth [26–28]. In conventional DeFi exchanges, AMMs like Uniswap determine prices based on a predefined function of supply and demand (e.g., constant product formulas), allowing users to trade assets without needing a direct counterparty order [29]. This property is highly attractive for illiquid LEM environments: an AMM can inherently mitigate extreme price swings and lack of trading counterparties by always providing a price quote from its liquidity pool. Recognizing these advantages, recent research has begun exploring AMM-based local energy markets. For instance, Bevin and Verma [30] develop a decentralized LEM model using an AMM, illustrating the potential for continuous market making in energy systems.

Such early energy-focused AMMs, however, typically import designs directly from financial cryptocurrency markets and thus face several shortcomings [31]. First, classical AMM protocols [29,32] assume continuous trading and immediate liquidity, which is misaligned with the periodic batch nature of electricity markets (e.g., hourly or 15-minute intervals). Energy supply and demand are cyclic and time-coupled, so a naively applied AMM may yield inefficient or unstable prices if it cannot clear trades in sync with these cycles. To address these limitations, several studies in the DeFi literature have explored the integration of batch execution with AMM-based pricing.

In this regard, Aldrich and López Vargas [33] experimentally demonstrate that frequent batch auctions reduce predatory trading, lower transaction costs, and decrease spread volatility compared to continuous double auctions, providing evidence for the benefits of discrete-time clearing. Ramseyer et al. [34] study the augmentation of batch exchanges with constant function market makers, showing how AMM liquidity pools can coexist with limit orders in a batch settlement to improve price discovery and computational tractability. Mohan [35] provides a comprehensive taxonomy of AMM exchange functions—including constant product, constant mean, and hybrid variants—that underpin algorithmic price formation in decentralized exchanges. Canidio and Fritsch [36] propose the function-maximizing AMM, which batches all trades and executes them at the post-batch marginal price, formally proving that batching is necessary to prevent order splitting and that competition among arbitrageurs guarantees equilibrium pricing. Building on these insights, our earlier work [37] conceptually demonstrated the potential of combining AMM-based pricing with batch settlement for energy trading environments without going deep into the design.

In addition, many existing P2P energy trading market designs in the literature simplify or neglect the modeling of physical networks—such as line capacity limits, voltage bounds, and loss allocation among market participants—governing power flows, leaving a gap in fully grid-integrated market design. While the blockchain-based P2P trading platforms presented in [38–40] incorporate electrical network constraints, these implementations typically perform load flow calculations and grid feasibility checks off-chain. Relying on off-chain computation (e.g., centralized servers or edge devices) to enforce network limits reduces the transparency and automation benefits of blockchain and introduces trust and privacy risks [41]. On the other hand, executing full AC power flow analysis on-chain is computationally prohibitive given current smart contract platforms. This has led to research on lightweight, approximated power-flow models suitable for on-chain execution [42,43]. Several P2P trading mechanisms employ simplified network models: some omit voltage drop calculations and focus only on balancing power flows [44–46]; others account for voltage but ignore line losses [47,48]. While these simplifications ease computation, they can compromise accuracy and reliability. Loss allocation is another challenge: losses may be divided equally among peers [49], allocated via power transfer distribution factors (PTDFs) [50], or assigned fixed coefficients [51]. These imprecise and ex-ante methods fail to reflect participants' actual contributions to losses and cannot capture cases where local trades reduce total system losses [52]. The on-chain power flow (OC-PF) formulation in [53] models voltage variations and allocates losses directly within smart contracts, representing progress toward decentralized grid-compliant trading, yet still approximates participant-level loss attribution. In summary, existing grid-aware mechanisms either rely on off-chain computation (reducing decentralization) or employ simplified on-chain models with partial fairness. Achieving a market that is both economically efficient and technically feasible remains an open challenge.

1.3. Contribution

To address the aforementioned research gaps, this work establishes a unified blockchain-based P2P energy trading architecture that combines liquidity-robust market design with network-aware on-chain settlement, ensuring both technical feasibility and economic viability in decentralized energy markets. To this end, an AMM-based batch auction (AMMBA) mechanism is proposed for P2P energy trading, where network constraints and loss allocation are explicitly modeled. Each participant determines its generation surplus or consumption deficit through a rule-based energy management process. After tokenization of energy and money in blockchain smart contracts, the AMMBA mechanism determines a single, uniform clearing price using a predefined pricing function to settle all transactions. To enhance market efficiency, a method is introduced for optimizing the parameters of the underlying pricing function, ensuring a balance between buyers' utility, sellers' profits, and demand–supply dynamics.

Regarding physical network modeling, distribution network security constraints are enforced on-chain using a simplified yet sufficiently accurate power flow calculation, ensuring that line flow and voltage limits are respected with minimal adjustments to participants' traded energy. Resulting power losses from local energy exchanges are fairly allocated among participants and incorporated into their traded energy prices, so that each agent is charged or rewarded according to its actual contribution to total system losses. Accordingly, the impact of distribution network modeling within the proposed AMMBA market mechanism is directly reflected in both the traded energy quantities and their corresponding prices.

Finally, the market mechanism is examined to satisfy incentive compatibility, budget balance, and individual rationality, ensuring economically sound operation. A prototype of the proposed blockchain-based market is implemented and evaluated through simulations on a low-voltage distribution network, benchmarked against traditional DA and uniform-price auction (UPA) mechanisms, involving several hundred residential participants.

In summary, this study provides the following contributions:

- An AMM-based batch auction mechanism design for illiquid, decentralized P2P energy trading that integrates batch-clearing with an automated, algorithmic market maker pricing approach.
- An on-chain modeling approach for distribution network constraints and fair allocation of power losses among market participants.
- Verification of incentive compatibility (IC) for the proposed mechanism by offering penalties to the market mechanism.
- A prototype implementation of the proposed network-constrained AMMBA as a blockchain-based smart contract, along with a simulation-based evaluation against traditional DA and UPA mechanisms using real-world data.

The remainder of this paper is structured as follows. The whole market framework including AMMBA market mechanism, on-chain network model and incentive analysis is introduced in Section 2. Section 3 presents the smart contract implementation of the proposed mechanism using the available data. The DA and UPA market setups are also provided for benchmarking to be evaluated by introduced Key Performance Indicators (KPIs). Section 4 discusses the benchmarking results and provides the individual performance analysis of the grid-aware AMMBA market mechanism. The conclusions and future work are given in Section 5, and four annexes are provided thereafter.

2. Proposed market framework

This section presents the market framework for a network-aware P2P energy trading model based on the AMMBA mechanism. As illustrated in Fig. 1, the framework operates in periodic market cycles and integrates three key components. First, a rule-based energy scheduling model determines each market participant's energy deficit or surplus, which in turn defines its role as a buyer or seller in each cycle. Second, the AMMBA market architecture is introduced, detailing the batch auction-based trading mechanism and the optimization model used to calibrate the pricing function for efficient and balanced market operation. Third, a distribution network modeling framework based on the OC-PF formulation is developed to enforce grid security constraints and allocate power losses resulting from P2P energy trades in a fair and transparent manner. Furthermore, the theoretical market mechanism properties of the proposed design are analyzed to ensure the robustness and practical viability of the AMMBA mechanism for LEMs.

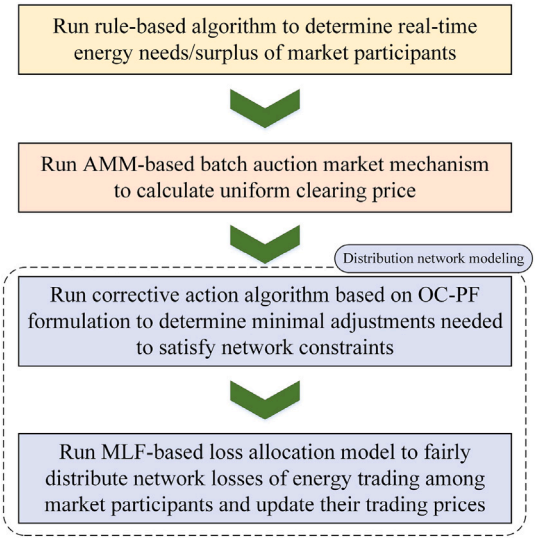

Fig. 1. General structure of the proposed network-constrained market framework.

2.1. Rule-based energy asset scheduling

The scheduling of energy assets for individual community members is performed using a rule-based energy management algorithm designed to ensure simplicity, transparency, and computational efficiency. Three types of energy assets are considered in this study including PV systems, home batteries, and EV chargers. A detailed description of the rule-based scheduling logic for these three types of energy assets is provided in Appendix A.

PV generation is used as the primary source to meet community member demand, with any surplus allocated to battery charging, EV charging, or market trading. The battery follows price-driven charging and discharging rules that consider electricity price forecasts, degradation costs, and technical constraints. It charges when prices are sufficiently low and expected to rise, and discharges when prices are high and expected to fall, while respecting rated power and state of energy constraints. If these conditions are not met, it remains idle. EV charging depends on the available plugged-in time and the required energy to reach the desired state of energy by departure. If charging needs exceed the available window, the EV charges continuously at rated power; otherwise, charging is shifted to lower-price intervals using a vehicle-specific price threshold.

Once the rule-based scheduling algorithm is applied to determine the operation of each energy asset, the resulting net demand profile of each community member—expressed as an aggregated surplus or deficit—is the only information communicated to the marketplace for trading. This aggregation of individual asset scheduling helps preserve participant privacy by preventing disclosure of detailed operational information while maintaining market transparency and trading efficiency.

2.2. AMMBA market architecture and design

After determining their energy deficit or surplus through the rule-based scheduling algorithm, community members (e.g., residential and commercial participants) participate in the AMMBA trading market to either procure the energy they need or sell their excess generation, acting as buyer or seller agents, respectively. In the proposed design, energy trading is organized in discrete market cycles, and during each cycle, the AMMBA mechanism, which is implemented as a smart contract, facilitates interactions between participants through a liquidity pool and algorithmic price formation. As shown in Fig. 2, the full workflow proceeds through a sequence of tokenization, bidding, and clearing.

This figure illustrates that the process begins on the seller side: when a community member identifies an energy surplus, it notifies the smart contract, which then programmatically mints the corresponding number of energy tokens (e-tokens) and transfers them to the producer's wallet. Then, the smart contract opens a timed auction window. During this phase, buyer agents deposit money into the auction pool to fund their energy purchases, while seller agents submit their e-tokens for sale. All incoming money and e-tokens are collected and held together in the smart contract, a process referred to as batching.

In the final phase, the smart contract determines a single, uniform clearing price for the cycle using a predefined AMM price function based on the total ratio of money to e-tokens in the batched pool. Once the auction window closes, the contract simultaneously settles all transactions by transferring money to the producers and the corresponding share of e-tokens to the consumers. Finally, consumers can use their received e-tokens to redeem the equivalent amount of physical energy. Afterwards, the liquidity pool is cleared for the next batch auction cycle, so unlike classical AMM models that maintain permanent liquidity, this mechanism utilizes the pool temporarily. In the following, we detail the AMMBA pricing function as well as the mechanisms used to allocate sellers' energy surplus and buyers' energy demand.

As stated earlier, within the LEM paradigm, seller and buyer agents are able to trade energy at prices above the FiT and below the retail price, enabling prosumers to increase their revenue while allowing consumers to reduce their energy costs. Accordingly, the pricing function must enforce these upper and lower boundaries: the clearing price cannot exceed the retail price, which would result in negative returns for consumers, nor fall below the FiT, which would impose losses on prosumers selling surplus energy. To this end, the sigmoid pricing function is selected for its smooth S-shaped curve, which ensures a gradual transition between the FiT and retail price, fosters market stability, and incentivizes participation by guaranteeing outcomes better than outside options. Additionally, this function captures the natural life-cycle of a growing market—with a slow start, a period of accelerated growth, and eventual saturation—providing a more realistic price dynamic than simpler linear or exponential models. Thus, the sigmoid pricing function determines the market clearing price based on the ratio of total deposited energy to total deposited money as follows.

$$\pi = f(M, E) = K_{\text{up}} - \frac{K_{\text{up}} - K_{\text{lo}}}{1 + e^{-B\left(\frac{E}{M} - \Theta\right)}} \tag{1}$$

where π represents the uniform clearing price, and K_{up} and K_{lo} are the upper and lower price limits, corresponding to the retail price and the FiT, respectively. M and E denote the total sum of money and energy that were deposited across all community members during a cycle, reflecting total market demand and supply. Two controlling parameters B and Θ are called steepness and midpoint of the sigmoid function and determine the behavior of the function. Following established approaches to energy pricing in P2P market mechanisms (e.g., Kim et al. [52]), we employ a sigmoid function to map the aggregate supply-to-demand ratio to a market clearing price. This functional form was chosen because it guarantees the resulting price strictly remains bounded within the economically meaningful interval between the FiT and the retail price. Additionally, its smooth, monotonic transition avoids volatile price jumps, offers intuitively interpretable parameters for the community, and satisfies the necessary mathematical conditions for incentive-compatibility.

To better illustrate the effects of the controlling parameters on the clearing price, Fig. 3(a) and (b) depict price function curves for different values of Θ and B, respectively. Fig. 3(a) demonstrates that increasing Θ shifts the transition point of the sigmoid pricing function to the left, meaning that the clearing price moves from K_{lo} to K_{up} at a lower demand-to-supply ratio. A higher Θ gives greater influence to producers, encouraging increased supply even under lower demand, whereas a lower Θ favors consumers by keeping prices closer to K_{lo} until higher

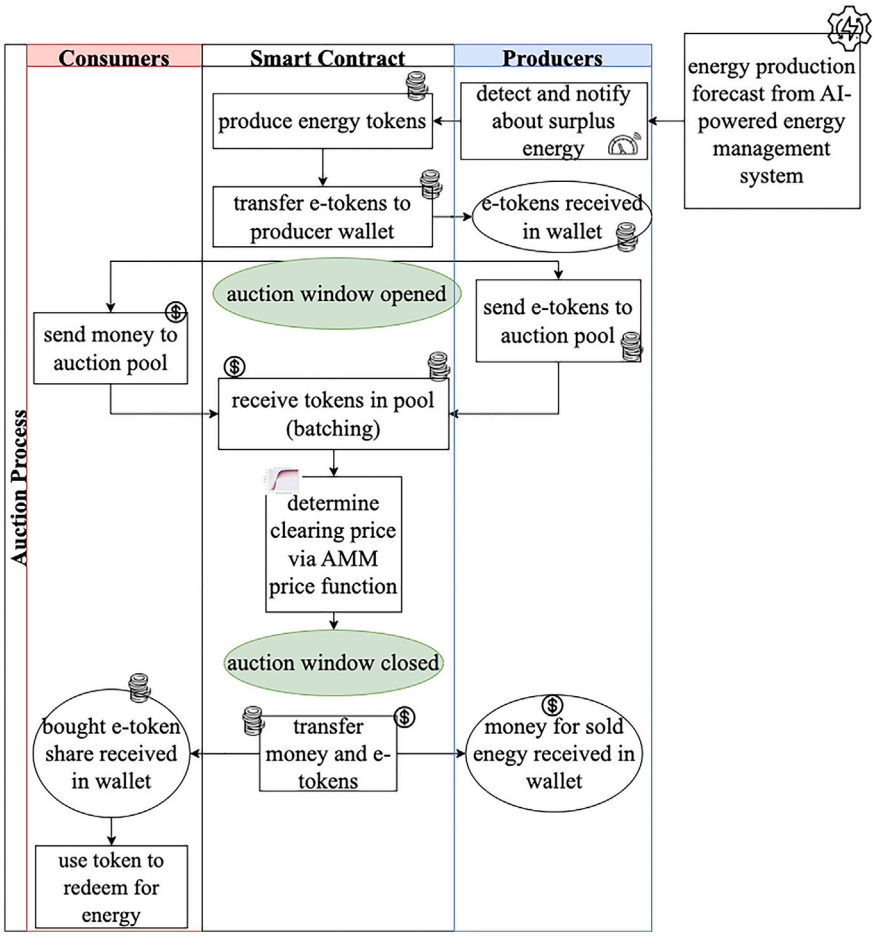

Fig. 2. AMMBA auction process.

demand levels are reached. Moreover, Fig. 3(b) illustrates the effect of the parameter B on the steepness of the price transition. Larger values of B create more abrupt price changes between K_{lo} and K_{up}, which can be advantageous in dynamic markets requiring rapid adjustments. Conversely, smaller B values result in smoother price transitions, leading to more stable clearing prices that may be preferable in markets favoring gradual adjustments.

As shown in Fig. 2, once the uniform clearing price is determined, the energy and funds are then distributed among participants at the end of the market cycle as follows: The energy received by each buyer is determined and adjusted based on their proportional share of the total deposited funds to ensure that they do not exceed the maximum energy they can afford based on their deposit and the price. If the costs allocated to each buyer according to their share exceed their deposit, the energy received is limited to the amount they can pay. This ensures that no buyer receives more energy than their deposited funds can cover. The formula for calculating the received amount of energy for a buyer agent i is defined as follows:

$$E_{\text{rec},i} = \min\left(\frac{M_i}{\pi}, E_{\text{total}} \times \frac{M_i}{M_{\text{total}}}\right) \tag{2}$$

where $E_{\text{rec},i}$ is the amount of energy received by buyer, π is the market clearing price, M_i is the amount of funds deposited by buyer i, E_{total} is the total energy available for distribution and M_{total} is the total money deposited by all buyers.

The earnings of a seller depend on the actual energy purchased by buyers, which is limited by the total funds they have deposited. If the buyers' funds are insufficient to purchase all the available energy, only a portion of the energy will be sold, and sellers can only be paid for that portion. The total energy sold E_{sold} is determined as the minimum of the total funds deposited by buyers divided by the price and the total energy available, ensuring it does not exceed what buyers can afford or what sellers can supply:

$$E_{\text{sold}} = \min\left(\frac{M_{\text{total}}}{\pi}, E_{\text{total}}\right) \tag{3}$$

Each seller's earnings M_j are then calculated based on the proportion of the total sold energy that comes from their own contribution, as follows.

$$M_j = \pi \times E_{\text{sold}} \times \frac{E_j}{E_{\text{total}}} \tag{4}$$

Finally, after distributing energy to buyers and payments to sellers, any remaining deposited money and unsold energy are returned to the respective participants. No energy or money tokens will be carried over to the next cycle in the AMM's liquidity pools.

As illustrated earlier, the controlling parameters of the pricing function, i.e., the steepness and midpoint, significantly influence the AMMBA market behavior. Therefore, identifying their optimal values is essential to ensure a fair balance between buyers and sellers. To measure the balance of the market, two essential indices are considered: **consumer utility** and **supplier profit**. More specifically, the goal of the optimization is to balance the utility and profit per transacted kWh for each consumer and producer at each market time window. In order to guarantee a dynamic price function responding to changes in

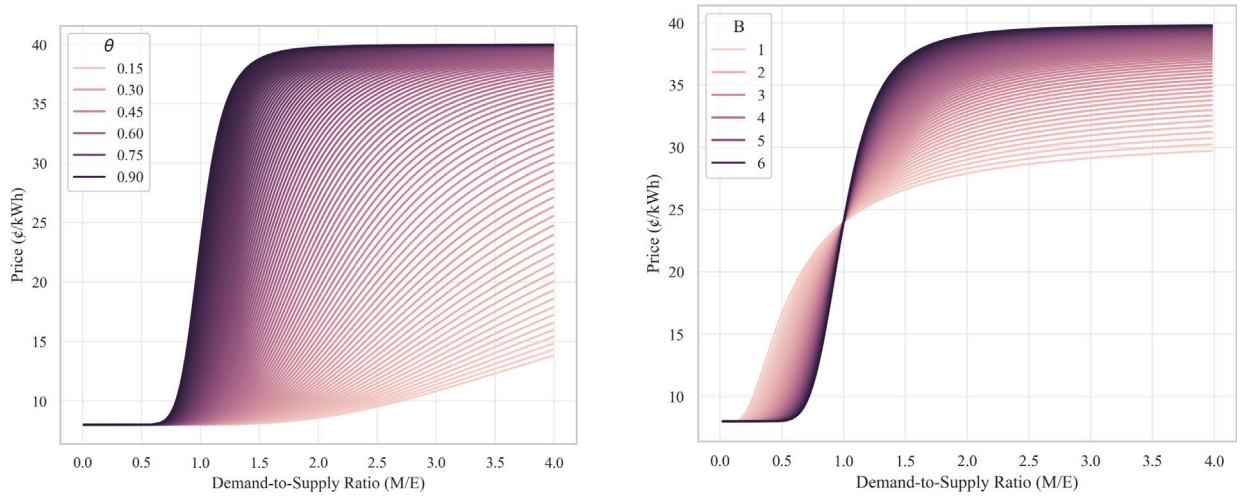

(a) The value of parameter B fixed at 10, (b) The parameter Θ fixed at 1,

Fig. 3. Impact of controlling parameters on the pricing function: (a) midpoint parameter, (b) steepness parameter.

supply-to-demand, a penalty term is formulated that becomes larger the more the price function deviates from the upper (lower) price limit at the lowest (highest) energy-to-money ratio. This ensures that the price function must transition from the upper to the lower price limit as the energy-to-money ratio increases.

The price function is adjusted to account for the variable retail prices provided in the dataset, while the FiT is assumed to remain fixed. Consequently, the uniform clearing price at time window t is given by (5).

$$\pi_t = f(M_t, E_t) = K_{\text{up},t} - \frac{K_{\text{up},t} - K_{\text{lo}}}{1 + e^{-B(\frac{E_t}{M_t} - \Theta)}} \tag{5}$$

Consumer utility is defined as the cost savings a consumer achieves by purchasing some or all of their energy demand through the LEM rather than buying it at retail price from the local energy supplier. Should a consumer receive more energy tokens than needed to cover their demand, it is assumed that the surplus energy is sold at a net loss for the FiT rate. The utility per kWh received from the consumer i at time window t is then given by (6).

$$U_{t,i} = \frac{E_{\text{rec},t,i}(K_{\text{up},t} - \pi_t) - \max(0, E_{\text{rec},t,i} - D_{t,i})(\pi_t - K_{\text{lo}})}{E_{\text{rec},t,i}} \tag{6}$$

where $E_{\text{rec},t,i}$ denotes the amount of energy tokens received by consumer i, and $D_{t,i}$ represents the energy demand of consumer i at time t. Furthermore, a **supplier profit** is defined as the additional revenue earned by selling surplus energy on the LEM rather than at the FiT rate. The profit per kWh sold by supplier j at time window t is given by (7).

$$P_{t,j} = \frac{E_{\text{sold},t,j}(\pi_t - K_{\text{lo}})}{E_{\text{sold},t,j}} = \pi_t - K_{\text{lo}} \tag{7}$$

where $E_{\text{sold},t,j}$ is the amount of energy tokens sold by seller j at time t.

The aim of the optimization is to determine the optimal midpoint and steepness parameters of the pricing function such that the minimum of the average profit per kWh of energy sold and the average utility per kWh of energy purchased at each time step is maximized, while penalizing static behavior of the pricing function. Accordingly, the objective function is defined as (8).

$$\max_{\{\Theta,B\}} \sum_t \left[\min\left(\frac{U_t}{I_t}, \frac{P_t}{J_t}\right) - \alpha \left(f(r_{\max}) - K_{\text{lo}} + K_{\text{up,t}} - f(r_{\min}) \right) \right] \tag{8}$$

where

$$U_t = \sum_i \frac{U_{t,i}}{E_{\text{rec},t,i}}; \quad P_t = \sum_j \frac{P_{t,j}}{E_{\text{sold},t,j}} \tag{9}$$

where I_t and J_t are the total number of consumers and suppliers at time t, $r_{\max}$ and $r_{\min}$ are the maximum and minimum energy-to-money ratios across all time windows. U_t and P_t are the average utility per kWh received and average profit per kWh sold at time t, respectively. The terms $f(r_{\max}) - K_{\text{lo}}$ and $K_{\text{up}} - f(r_{\min})$ in the optimization objective function represent the deviation of the price at the lowest energy-to-money ratio from the retail price and the deviation of the price at the highest energy-to-money ratio from the FiT, respectively. Further, the parameter α is the weight of the penalty term and can be adjusted to control the influence of the price deviations at maximum and minimum energy-to-money ratios on the optimization objective. Reducing α leads to a more stable price function, whereas increasing its value causes a more volatile price function. The optimization is carried out by applying the bounded limit-memory Broyden-Fletcher-Goldfarb-Shanno algorithm (L-BFGS) [54] which can be performed weekly, monthly or seasonally based on community manager observation on the rate of supply–demand changes.

In practice, the optimization of parameters would ideally be managed in a fully decentralized manner through a decentralized autonomous organization (DAO) consisting of all stakeholders, or alternatively, via a democratically elected community manager. DAOs are blockchain-based governance structures that enable collective decision-making without centralized control, typically relying on smart contracts to enforce rules and execute governance decisions [55]. Parameter adjustments would be conducted at regular intervals, guided by both historical consumption patterns and forecasted energy data, thereby ensuring continuous alignment with the evolving needs and preferences of the energy community.

A practical concern for any blockchain-based energy market is the cost and latency of on-chain transactions. On public Ethereum Layer 1, gas fees can reach several dollars per transaction, which would be prohibitive for the small-value energy trades typical in residential LEMs. However, residential energy communities are well-suited to *permissioned* or *Layer-2 (L2)* blockchain architectures where transaction fees are negligible or near-zero. Established examples include the Energy Web Chain—a Proof-of-Authority network designed specifically for energy applications [56]—as well as general-purpose L2 rollups such as Polygon PoS and Optimism, all of which enable transaction processing at costs

of only fractions of a cent. In a community-managed deployment, the blockchain would most naturally be operated as a permissioned network governed by the DAO described above, eliminating gas-market competition entirely. Block confirmation times on such networks are typically 1–3 s, well within the 15-minute settlement cycle of the proposed AMMBA mechanism. To ensure the smart contract security, the development follows established best practices including reentrancy guards, integer-overflow protection (using Solidity ≥ 0.8), and access-control modifiers that restrict settlement execution to the designated market-operator address.

2.3. On-chain distribution network modeling

The energy trading among prosumers and consumers, as determined by the proposed AMMBA market framework, is physically constrained by the underlying distribution network. Therefore, accurately modeling the network security constraints and fairly allocating network costs (such as power losses) are crucial to ensure feasible and reliable market outcomes. Modeling these aspects directly on-chain, alongside the AMMBA market architecture, enhances transparency, trust, and automation in the grid-aware local energy trading process.

To address these issues, this section first presents an OC-PF formulation for radial distribution networks, a computationally efficient method that can be directly implemented in smart contracts. Using the OC-PF model, we then formulate a corrective action algorithm that determines the minimal consumption/generation adjustments required to satisfy distribution network operational limits in AMMBA energy exchange, and propose a fair loss allocation scheme for market participants, all implemented entirely on-chain. It should be noted that, in the network-related analyses presented below, smart meter measurement errors and feeder parameter variations are assumed to be negligible and are therefore not explicitly modeled.

2.3.1. Network security constraints

In this study, feeder power flow and node voltage magnitude limits are considered as the primary distribution network security constraints. To properly incorporate these constraints into the market framework, a corrective action optimization algorithm is systematically formulated and executed to determine the minimal demand reduction of buyer agents or generation curtailment of seller agents required to ensure network feasibility and secure operation. Accordingly, the algorithm computes the optimal adjustments corresponding to the energy exchanges determined by the AMMBA mechanism; when violations occur, the necessary corrective actions are enforced, whereas in the absence of violations, the optimization naturally yields zero adjustment, thereby preserving the original market outcome.

To this end, a power flow model is required that can be implemented directly within on-chain smart contracts while still providing sufficiently accurate calculations of node voltage magnitudes and feeder power flows. In AC power flow equations, the main nonlinearity arises from feeder losses, which significantly increase the computational cost. As shown in Appendix B.1, by introducing suitable virtual variables, the loss-related term can be eliminated, allowing feeder power flows to be expressed as linear functions of the virtual variables corresponding to nodal injections, as follows.

$$\mathbf{F}^{p,*} = \mathbf{A}_f\,\mathbf{P}^*, \quad \mathbf{F}^{q,*} = \mathbf{A}_f\,\mathbf{Q}^* \tag{10}$$

where $\mathbf{A}_f$ is a binary matrix indicating whether the power consumption at a given node is routed through a specific feeder (1 if it does, 0 otherwise). Here, $\mathbf{P}^*$ and $\mathbf{Q}^*$ denote the virtual active and reactive net power consumption vectors of all nodes, while $\mathbf{F}^{p,*}$ and $\mathbf{F}^{q,*}$ represent the virtual active and reactive power flow vectors of all feeders. These vectors are obtained as follows.

$$\mathbf{P}^* = \mathbf{P} \oslash \mathbf{V}, \quad \mathbf{Q}^* = \mathbf{Q} \oslash \mathbf{V} \tag{11}$$

$$\mathbf{F}^{p,*} = \mathbf{F}^{p} \oslash \mathbf{V}_{par}, \quad \mathbf{F}^{q,*} = \mathbf{F}^{q} \oslash \mathbf{V}_{par} \tag{12}$$

where the operator ⊘ denotes element-wise division. $\mathbf{P}$ and $\mathbf{Q}$ represent the active and reactive power consumption vectors of all nodes, while $\mathbf{F}^p$ and $\mathbf{F}^q$ denote the active and reactive power flow vectors of all feeders, respectively. Additionally, $\mathbf{V}$ and $\mathbf{V}_{par}$ represent the voltage magnitude vector of all nodes and the vector of parent-node voltage magnitudes associated with each feeder, respectively.

In addition, based on the mathematical derivations presented in Appendix B.2, the voltage magnitudes of all nodes can be computed as a linear function of the virtual power flow variables, as follows.

$$\mathbf{V} = \mathbf{V}_1 - \mathbf{H}_v(\mathbf{r} \odot \mathbf{F}^{p,*}) - \mathbf{H}_v(\mathbf{x} \odot \mathbf{F}^{q,*}) \tag{13}$$

where the operator ⊙ represents element-wise multiplication, $\mathbf{H}_v$ denotes the path matrix for all nodes of the network, $\mathbf{r}$ and $\mathbf{x}$ are the vectors of resistance and reactance for all feeders, respectively, and $\mathbf{V}_1$ is the voltage magnitude vector of the reference node (node 1). Thus, by incorporating (10), (11), and (13), and eliminating the virtual variables, the OC-PF model can be compactly expressed in the following formulation.

$$\mathbf{V} = \mathbf{V}_1 - \mathbf{H}_v\big(\mathbf{r} \odot \mathbf{A}_f(\mathbf{P} \oslash \mathbf{V})\big) - \mathbf{H}_v\big(\mathbf{x} \odot \mathbf{A}_f(\mathbf{Q} \oslash \mathbf{V})\big) \tag{14}$$

To solve this equation, an iterative procedure is employed. The algorithm starts with an initial guess for the nodal voltage magnitudes (e.g., 1.0 p.u.). At each iteration, the updated voltage vector $\mathbf{V}$ is computed using (14), and the process is repeated until convergence is reached, i.e., when successive iterations result in negligible changes in $\mathbf{V}$. Once convergence is achieved, the voltage magnitudes of all nodes are obtained, and the power flows through all feeders are subsequently computed using (10), (11), and (12).

Using the OC-PF model described above, we develop a corrective action algorithm that is systematically executed to determine the required adjustments in buyer agents' consumption or seller agents' generation to satisfy distribution network security constraints. To this end, an optimization problem is formulated to enforce nodal voltage magnitudes and feeder power flows within predefined limits with the smallest possible corrective adjustments as follows.

$$\min_{\Delta\mathbf{P}} \quad \Delta\mathbf{P}^\top \Delta\mathbf{P} \tag{15}$$

$$\text{subject to:} \quad \mathbf{F}^p_{\min} \le \mathbf{F}^p_{\text{AMMBA}} - \mathbf{S}_f\,\Delta\mathbf{P} \le \mathbf{F}^p_{\max}, \quad (\bar{\lambda}, \underline{\lambda}) \tag{16}$$

$$\mathbf{V}_{\min} \le \mathbf{V}_{\text{AMMBA}} + \mathbf{S}_v\,\Delta\mathbf{P} \le \mathbf{V}_{\max}, \quad (\bar{\mu}, \underline{\mu}) \tag{17}$$

$$\mathbf{P}_{\min} \le \Delta\mathbf{P} \le \mathbf{P}_{\max} \tag{18}$$

The objective function (15) aims to minimize the total squared corrective adjustments of consumption and generation across all agents, ensuring that the applied corrections are as small as possible while restoring network feasibility. Here, $\Delta\mathbf{P}$ denotes the vector of corrective adjustments for all agents. The corrective adjustments ensure that the feeder power flows and node voltages remain within their allowable limits, as enforced by constraints (16) and (17). In these equations, $\mathbf{F}^p_{\min}$ and $\mathbf{F}^p_{\max}$ denote the minimum and maximum allowable power flows through all feeders, while $\mathbf{V}_{\min}$ and $\mathbf{V}_{\max}$ denote the minimum and maximum allowable voltage magnitudes at all nodes. $\mathbf{F}^p_{\text{AMMBA}}$ and $\mathbf{V}_{\text{AMMBA}}$ correspond to the feeder power flows and node voltages resulting from the AMMBA-based energy exchanges. Finally, constraint (18) bounds the corrective adjustments for all agents. The adjustments for buyer agents are limited between zero and their initially allocated consumption, while the adjustments for seller agents are limited between their initially allocated generation (negative values) and zero, ensuring that all corrective actions remain physically feasible.

In the above, $\mathbf{S}_f$ and $\mathbf{S}_v$ denote the matrices of power transfer sensitivity factors for all feeders and the voltage transfer sensitivity factors for all nodes, respectively, with respect to adjustments in buyer agents' consumption and seller agents' generation. These sensitivity matrices are computed in (19) and (20) using the OC-PF model.

$$\mathbf{S}_f = (\mathbf{V}_{par} \odot_c \mathbf{A}_f \oslash_r \mathbf{V})\mathbf{C}_{an} \tag{19}$$

$$\mathbf{S}_v = \mathbf{H}_v(\mathbf{r} \odot_c \mathbf{A}_f \oslash_r \mathbf{V})\mathbf{C}_{an} \tag{20}$$

where operators $\odot_c$ and $\oslash_r$ denote column-wise and row-wise broadcasted element-wise multiplication and division, respectively. $\mathbf{C}_{an}$ represents the agent-to-node mapping matrix, which specifies the network node associated with each market agent (1 if the agent is connected to that node, 0 otherwise). The above sensitivity factor relations indicate that, in addition to the network topology and the agents' connection points, the sensitivity matrices also depend on the node voltage magnitudes.

To solve the optimization problem described above in a decentralized manner, it is decomposed into independent subproblems for each agent, exploiting the linearity of the constraints and separable objective. The details of the solution method, including the Lagrangian function, the update rules for the dual variables, and the convergence conditions, are provided in the Appendix C. Finally, each agent determines its optimal corrective adjustment at each iteration based on the current dual variables penalizing constraint violations. The closed-form solution for each agent is given by:

$$\Delta P_i = \min\left(P_{i,\mathrm{AMMBA}}, \max\left(0, -\frac{\phi_i}{2}\right)\right), \quad \forall \text{buyer } i \tag{21}$$

$$\Delta P_j = \max\left(P_{j,\mathrm{AMMBA}}, \min\left(0, -\frac{\phi_j}{2}\right)\right), \quad \forall \text{seller } j \tag{22}$$

$$\boldsymbol{\phi} = \mathbf{S}_f^{\top}(\bar{\lambda} - \underline{\lambda}) + \mathbf{S}_v^{\top}(\bar{\mu} - \underline{\mu}) \tag{23}$$

where $P_{i,\mathrm{AMMBA}}$ and $P_{j,\mathrm{AMMBA}}$ represent the initially allocated buyer agent's consumption and seller agent's generation, respectively, and $\boldsymbol{\phi}$ denotes the vector of aggregated sensitivity-weighted dual variables that capture the impact of network constraint violations on each agent's corrective adjustment. Once the Lagrangian Relaxation (LR) method converges by satisfying the convergence criteria, the OC-PF is resolved with the applied corrective adjustments to update the node voltage magnitudes and, consequently, to recompute the $\mathbf{S}_f$ and $\mathbf{S}_v$ matrices, as illustrated in (19) and (20). This outer iterative process continues until the convergence criterion, defined as a negligible variation in node voltages between successive iterations, is satisfied. Finally, the resulting consumption and generation adjustments are applied to all agents, and their energy exchanges are updated accordingly.

2.3.2. Loss allocation mechanism

Power losses resulting from energy exchanges among LEM participants can be either positive, meaning that total network losses increase, or negative, indicating that the exchanges contribute to a reduction in total losses. In this study, the corresponding costs or benefits in both cases are fairly allocated among market participants according to their respective contributions, such that the resulting loss-related costs or benefits are directly reflected in their traded energy prices. Compared to many existing studies that rely on fixed empirical coefficients or purely volume-based schemes, the proposed approach provides a more accurate and physically meaningful allocation. To this end, marginal loss factors (MLFs) are calculated for all nodes, reflecting how an incremental change in power withdrawal at each node impacts the total network losses.

To begin, the network loss formulation is derived, followed by the computation of MLFs for all nodes. In the OC-PF model, network losses can be calculated as follows, with a detailed derivation provided in the Appendix D.1.

$$\mathbf{P}^{\mathrm{loss}} = \mathbf{P}^{\top}(\mathbf{1} \oslash \mathbf{V} - \mathbf{1}) \tag{24}$$

Considering the mathematical analysis provided in the Appendix D.2, the MLF vector $\boldsymbol{\Gamma}$—representing the derivative of the total network losses with respect to the power consumption of all nodes—can be computed as follows.

$$\boldsymbol{\Gamma} = (\mathbf{1} \oslash \mathbf{V} - \mathbf{1}) - \mathbf{D}\left(\mathbf{P} \oslash \mathbf{V}^{\odot 2}\right) \tag{25}$$

$$\mathbf{D} = \frac{-\mathbf{H}_v(\mathbf{r} \odot_c \mathbf{A}_f \oslash_r \mathbf{V})}{\mathbf{I} - \mathbf{H}_v\left(\mathbf{r} \odot_c \mathbf{A}_f \odot_r (\mathbf{P} \oslash \mathbf{V}^{\odot 2})\right) + \mathbf{H}_v\left(\mathbf{x} \odot_c \mathbf{A}_f \odot_r (\mathbf{Q} \oslash \mathbf{V}^{\odot 2})\right)} \tag{26}$$

After computing $\boldsymbol{\Gamma}$, each node's MLF value is interpreted to indicate how the consumption or generation at that node affects network losses. A positive MLF indicates that an incremental increase in consumption at the corresponding node increases network losses, whereas an incremental increase in generation reduces losses. Conversely, a negative MLF implies that an incremental increase in consumption decreases network losses, while an incremental increase in generation increases losses. Based on the sign of the network losses resulting from energy exchanges, the associated costs or benefits are allocated accordingly. In the case of positive losses, the cost is allocated to agents contributing to the increase in network losses, namely buyer agents at nodes with positive MLFs and seller agents at nodes with negative MLFs. On the other hand, if the power loss is negative, the benefit is allocated to agents contributing to the reduction of network losses, namely seller agents at nodes with positive MLFs and buyer agents at nodes with negative MLFs.

Once it is determined which market participants are responsible for the cost or benefit associated with the network losses caused by energy exchanges, each participant's individual share is computed based on their contribution. Specifically, it is calculated as the product of their MLF and their respective consumption or generation, and then normalized among all agents involved in the loss allocation. The resulting normalized value represents each agent's proportional share of the cost or benefit associated with network losses, with the cost or benefit being evaluated at the appropriate price: retail electricity price for positive network losses and FiT for negative network losses. This cost or benefit is then combined with the cost or revenue associated with the energy exchanged by buyer and seller agents, and the resulting total amount is subsequently divided by the traded energy quantity to determine the final energy exchange price for each participant. Consequently, in the case of positive losses, the associated cost increases the energy price for buyers and decreases it for sellers that contribute to loss increases, while in the case of negative losses, the associated benefit reduces the price for buyers and increases it for sellers that contribute to loss reductions. This approach ensures that the total cost or benefit is fairly and proportionally distributed according to each participant's impact on the network losses.

To summarize, the proposed on-chain distribution network modeling integrated into the AMMBA energy trading framework, including network security constraints and loss allocation, is illustrated in Algorithm 1. The algorithm provides a step-by-step workflow for adjusting the consumption and generation of buyer and seller participants as corrective actions to alleviate network constraint violations, while also fairly allocating the costs or benefits associated with network losses resulting from participants' energy trading.

2.4. Market mechanism properties

In this section, some definitions are introduced to ensure the right incentives of market participants as *Incentive Compatibility* (IC) for the AMMBA mechanism. It is supposed that the mechanism sets a uniform price $p_t = f(M_t, E_t) \in [K_{\mathrm{lo}}, K_{\mathrm{up},t}]$ and the pro-rata batching allocation.

2.4.1. Setup and notation

Assume there is a cycle (market window) t where buyers i deposit $M_{t,i} \geq 0$, and sellers j report $E_{t,j} \geq 0$. Define aggregate money and energy:

$$M_t = \sum_i M_{t,i}, \quad E_t = \sum_j E_{t,j}$$

Algorithm 1 Integrated corrective action and loss allocation procedure.

Stage 1: Corrective Actions for Grid Constraint Violation Alleviation
Run OC-PF to compute node voltages $\mathbf{V}$ and feeder flows $\mathbf{F}^p$ and $\mathbf{F}^q$
if any deviation from network limits is detected **then**
  Initialize iteration counter: $k \leftarrow 0$
  while convergence criteria are not satisfied **do**
    Compute $\mathbf{S}_f^{(k)}$ and $\mathbf{S}_v^{(k)}$ using Eqs. (19)–(20)
    Run the LR-based decentralized optimization model and compute optimal consumption and generation adjustments $\Delta\mathbf{P}^{(k)}$
    Update all participants' energy exchange, update nodal net demands, and rerun OC-PF
    Using updated node voltages $\mathbf{V}^{(k+1)}$, update $\mathbf{S}_f^{(k+1)}$, $\mathbf{S}_v^{(k+1)}$
    $k \leftarrow k+1$
  end while
else
  No corrective action required
end if
Stage 2: Loss Allocation among Market Participants
Compute power losses caused by energy exchanges using Eq. (24)
Determine the monetary impact: apply the retail price for positive losses and the FiT for negative losses
Calculate marginal loss factor (MLF) vector $\mathbf{\Gamma}$ using Eqs. (25) and (26)
if network losses caused by energy exchange is positive **then**
  Group participants contributing to *increasing* losses (positive-loss): buyers at nodes with $\Gamma > 0$ and sellers at nodes with $\Gamma < 0$
else
  Group participants contributing to *decreasing* losses (negative-loss): sellers at nodes with $\Gamma > 0$ and buyers at nodes with $\Gamma < 0$
end if
for each participant in the relevant group **do**
  Compute contribution as the product of the node's MLF value and the participant's traded energy
  Normalize contributions among all selected participants
  Allocate proportional share of total cost/benefit
  Compute the final price by combining the allocated loss cost/benefit with each participant's energy trading revenue or cost
end for
Output: Network-feasible consumption/generation schedule and final loss-allocated energy exchange price for each participant

Realizing the uniform price $p_t = f(M_t, E_t)$, define the aggregate cleared quantity:

$$Q_t \equiv \min\left\{\frac{M_t}{p_t}, E_t\right\}.$$

A round is **supply-limited** if $Q_t = E_t$ and **demand-limited** if $Q_t = M_t/p_t$ (uniquely determined by (M_t, E_t) since f is single-valued). Smart meters provide measured demand $D_{t,i}$ and deliverable surplus $A_{t,j}$. A deadband $\eta_t \geq 0$ shields small exogenous grid adjustments.

Pro-rata allocations are $q_{t,i}$ (buyer i's received energy) and $s_{t,j}$ (seller j's sold energy). Pre-penalty payoffs are:

$$u_{t,i}^{\text{buy}} = (K_{\text{up},t} - p_t)\,\min\{q_{t,i}, D_{t,i}\} - (p_t - K_{\text{lo}})\,[q_{t,i} - D_{t,i}]_+,$$
$$u_{t,j}^{\text{sell}} = (p_t - K_{\text{lo}})\,s_{t,j}.$$

Penalty terms – Economically, we try to eliminate any incentive to exercise market power (like a buyer's monopoly power or a seller's monopoly power) – effectively forcing everyone to behave as price-takers. The mechanism introduces two types of penalties to achieve this: *shortfall penalties* to punish infeasible over-reporting, and *externality penalties* (EP) to neutralize profitable price manipulation, grounded in the Vickrey-Clarke-Groves (VCG) theory [57,58]:

Shortfall penalty (feasibility). The shortfall penalty $\Phi(t, j)$ applies if seller j fails to deliver the energy they claimed. If a seller reports $E(t, j)$ but can only actually supply $A(t, j)$ (as measured by the smart meter), any shortfall beyond a small tolerance η_t is penalized. Formally:

$$\Phi_{t,j} = K_t^{\text{sho}}\left[s_{t,j} - A_{t,j} - \eta_t\right]_+, \qquad K_t^{\text{sho}} = \gamma\, K_{\text{up},t},\ \ \gamma > 1. \tag{27}$$

Here $[x]_+$ means the positive part of x (zero if x is negative) and η_t is designed to provide a buffer for noise or small deviations e.g., caused by PF corrective action for grid security explained in Section 2.3. So if a seller's allocated sale $s(t, j)$ exceeds their actual deliverable $A(t, j)$ by more than η_t, they pay a fine on each undelivered kWh. Importantly, $K_t^{sho} = \gamma K_{up,t}$ is set above the maximum possible price ($\gamma > 1$), meaning the penalty per kWh of shortfall exceeds even the highest revenue per kWh the seller could have earned. The penalty is imposed **ex-post** and eliminates any incentive for *over-reporting* supply.

Externality penalties (EP). A seller might withhold some of their energy to drive the price up in a *supply-limited* round, or a buyer might strategically under-fund to drive the price down in a *demand-limited* round. These behaviors create negative externalities: one agent's misreport distorts the price and harms the other side of the market. The mechanism addresses this through *EP*, which charges an agent for the harm their misreport caused to others.

The EP is only applied in the regime where an agent can influence the price: sellers are only penalized for withholding in *supply-limited* rounds, and buyers are only penalized for under-funding in *demand-limited* rounds.

- Sellers in **supply-limited rounds** – *Withheld energy* is the difference between what a seller could have supplied and what they actually sold. Using the smart meter data, the withheld amount for seller j is:

  $$W_{t,j}^{\text{sell}} = \left[A_{t,j} - s_{t,j} - \eta_t\right]_+.$$

  i.e., the surplus energy the seller had available $A(t, j)$ but didn't supply. If seller j hadn't withheld that energy, the total supply in the round would have been higher. Thus, the counterfactual price to gauge the price impact of that withholding is:

  $$p_{t,j}^{\text{cf,sell}} = f\big(M_t,\ E_t + W_{t,j}^{\text{sell}}\big)$$

  This is the price that would have resulted if seller j had truthfully supplied those withheld units. The penalty formula for seller j is then given by (28):

  $$\phi_{t,j}^{\text{sell}} = \underbrace{(p_t - p_{t,j}^{\text{cf,sell}})\,Q_t}_{\text{harm to others}} \cdot \mathbf{1}\{Q_t = E_t\}. \tag{28}$$

  Harm to others is essentially the total extra amount consumers paid due to the higher price, compared to the counterfactual where j didn't withhold. This penalty forces a withholding seller to pay for the negative externality they caused.
- Buyers in **demand-limited rounds.** A strategic buyer might try to under-report their true demand or budget in a *demand-limited* round in order to lower the price. First, we define the buyer's unmet need due to under-reporting. The buyer's unmet demand (kWh not received) is:

  $$W_{t,i}^{\text{buy}} = \left[D_{t,i} - q_{t,i}\right]_+.$$

  If $W_{t,i}^{\text{buy}} > 0$, it suggests that buyer i could have bought more energy if they were willing to spend more. We then consider a counterfactual scenario where buyer i had funded those extra $W_{t,i}^{\text{buy}}$ (kWh) at the realized price. We add $\Delta M_{t,i} = p_t\, W_{t,i}^{\text{buy}}$ to M_t while holding E_t

fixed, and recompute:

$$p_{t,i}^{\text{cf,buy}} = f\big(M_t + \Delta M_{t,i},\ E_t\big).$$

This $p_{t,i}^{\text{cf,buy}}$ is the hypothetical new price if buyer i had invested the additional funds to cover their unmet demand. The Buyer's penalty is defined as (29):

$$\phi_{t,i}^{\text{buy}} = \underbrace{(p_{t,i}^{\text{cf,buy}} - p_t)\,Q_t}_{\text{harm to others}} \cdot \mathbf{1}\{Q_t = M_t/p_t\}. \tag{29}$$

Harm to others is the increase in price caused by buyer i's underfunding, times the quantity Q_t that was traded. This represents the total revenue loss to the sellers because the price was kept lower than it should have been.

2.4.2. Incentive Compatibility (IC)

Lemma 1 (Seller Incentive Compatibility). *For any seller j:*

(a) Over-reporting is strictly unprofitable.
(b) Withholding in supply-limited regimes is unprofitable.

Proof. of Lemma 1 Part (a) follows directly from the shortfall penalty design in (27). For each undeliverable kWh, the seller is charged $K_t^{\text{sho}} > K_{\text{up},t} \geq p_t$, exceeding their maximal revenue per unit. Thus, over-reporting yields strictly negative net utility.

Part (b): In supply-limited regimes, under-reporting (withholding) may raise the price. Let $p_{t,j}^{\text{cf,sell}}$ denote the price had seller j fully reported. Then by monotonicity of f, $p_{t,j}^{\text{cf,sell}} = f(M_t, E_t + W_{t,j}^{\text{sell}}) \leq p_t$. The seller's gain from this price increase is limited to their own sold volume: Gain $= (p_t - p_{t,j}^{\text{cf,sell}})s_{t,j}$. The penalty (28) charges the total external harm: Penalty $= (p_t - p_{t,j}^{\text{cf,sell}})Q_t$. Since an individual seller's volume cannot exceed the total market volume ($s_{t,j} \leq Q_t$), the penalty is strictly greater than or equal to the gain. Hence, the net benefit from under-reporting is non-positive. □

Lemma 2 (Buyer Incentive Compatibility). *For any buyer i:*

(a) Over-funding is strictly suboptimal or payoff-neutral.
(b) Under-funding in demand-limited regimes reduces net payoff.

Proof. of Lemma 2 Part (a): Contributing more than $p_t D_{t,i}$ either raises the clearing price or results in excess allocation sold at K_{lo} which is a weakly worse outcome.

Part (b): In demand-limited regimes, reducing $M_{t,i}$ below $p_t D_{t,i}$ decreases one's allocation but might lower the price. Let $p_{t,i}^{\text{cf,buy}} = f(M_t + p_t W_{t,i}^{\text{buy}}, E_t) \geq p_t$ be the counterfactual price had the buyer funded the full amount. The buyer's gain from the price decrease is limited to their allocation: Gain $= (p_{t,i}^{\text{cf,buy}} - p_t)q_{t,i}$. The penalty (29) charges the total external harm: Penalty $= (p_{t,i}^{\text{cf,buy}} - p_t)Q_t$. Since an individual buyer's allocation cannot exceed the total market volume ($q_{t,i} \leq Q_t$), the penalty is strictly greater than or equal to the gain. Thus, under-funding reduces utility. □

Theorem 1 (Dominant-Strategy Incentive Compatibility). *Under the AMMBA mechanism, truthful reporting is a dominant strategy for all participants in every round. Specifically, it is strictly optimal for:*

- *each buyer i to fund their true metered demand, i.e., $M_{t,i} = p_t D_{t,i}$*
- *each seller j to report their true deliverable surplus, i.e., $E_{t,j} = A_{t,j}$*

This holds regardless of a participant's potential price impact, due to the enforcement of regime-sensitive externality penalties and the strict penalty on infeasible overstatements.

Proof of Theorem 1. Lemmas 1 and 2 together eliminate all profitable unilateral deviations: over-reports are strictly penalized (seller side), and regime-specific misreports (withholding or under-funding) are countered by penalties that strictly exceed the marginal benefits of price manipulation. Thus, truthful reporting strictly dominates all unilateral strategies. □

The dominant-strategy IC results established above apply to *individual* agents acting independently. A natural extension is to ask whether a *coalition* of sellers could jointly withhold supply to raise the clearing price in a coordinated manner. Under the AMMBA mechanism, coordinated withholding by a coalition $\mathcal{S}'$ of sellers would increase the price (since E decreases and M is held fixed, shifting the supply-to-demand ratio downward). However, the externality penalty is applied to each individual seller based on their personal withheld volume and the resulting price impact; it does not scale with the size of the coalition. Consequently, while individual defection is dominated by truthful reporting under the VCG-style penalty, the mechanism does not currently provide formal coalition-proofness guarantees. This limitation is shared by most practical AMM and DA designs in the literature [59]. Extending the penalty structure to coalition-aware mechanisms—for instance, through a Pigouvian tax on measured net supply deviations at the community level—is an important direction for future work and is feasible within the smart-contract framework since only aggregate supply and individual deviations need to be observed.

3. Market simulation setup

3.1. Data and implementation setup

The simulation uses a dataset published by Faia et al. [60] that contains high-resolution energy consumption and PV generation, as well as detailed home battery and EV characteristics. This dataset is based on real-world data for 250 households, with consumption profiles derived from public data in the United Kingdom and France [61], generation profiles synthesized from actual PV data, and pricing reflecting Portuguese power tariffs [62]. Using this dataset as a reference, a synthetic dataset for 1000 households was generated by statistically scaling and diversifying the original profiles, preserving temporal patterns and realistic correlations across consumption, PV generation, and other energy assets. To avoid overfitting during AMMBA parameter optimization, data for four days were generated: three days for price function parameter tuning and one day for out-of-sample evaluation.

The original dataset includes PV profiles for 200 households, BESSs for 150 households, and EVs for 100 households. This corresponds to an approximate 86% prosumer penetration. To evaluate the performance of the proposed model under different prosumer participation, three scenarios with decreasing levels of prosumer penetration are considered. These scenarios are detailed in Table 1 with an hourly depiction on demand and supply in Fig. 4.

In addition to energy consumption and generation profiles and the characteristics of available energy assets, the dataset provides a time-varying retail price and a fixed FiT. Fig. 5 visualizes both the retail price and the FiT, representing the upper and lower bounds for the sigmoid pricing function.

In addition, the IEEE 33-node radial distribution network is used as the test system under study. The peak load of the original test system is 3715 kW, and to model the temporal variations of the load, a standard load profile (shown in Fig. 6) is applied. To account for the addition

Table 1
Different simulation scenarios.

Scenario	Number of prosumers	Number of consumers	Prosumer penetration	Total demand (kWh)*	Total surplus (kWh)
Low	291	709	29%	32,483	7105
Medium	565	435	56%	32,483	13,400
High	856	144	86%	32,483	20,118

*Only includes periods with surplus energy production.

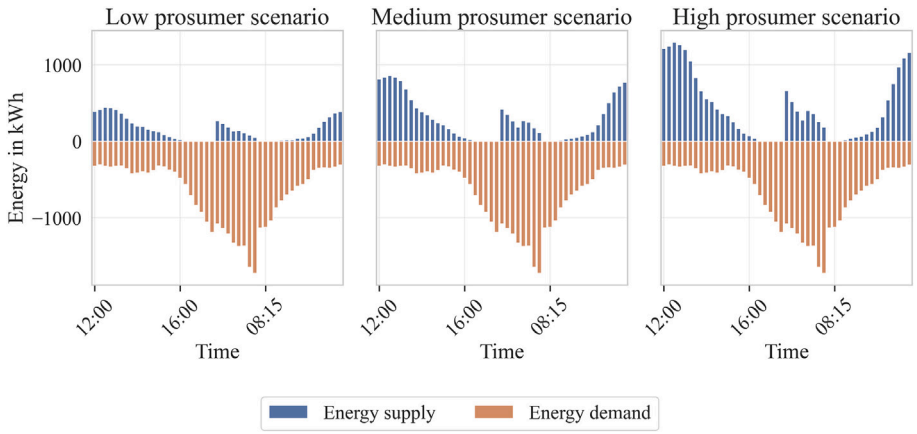

Fig. 4. Energy production and generation of the simulation scenarios.

of 1000 new households, the original active and reactive base loads of the network are multiplied by 0.85, and the households are distributed across the nodes as follows: households 1–8 are connected to node 2, while nodes 3–33 each host 32 households, as illustrated in Fig. 6. The allowable voltage range of test system is $[0.9, 1.1]$, and although no explicit line flow limits are specified, appropriate constraints are assumed in the simulations to demonstrate the performance of the proposed model.

3.1.1. Smart contract implementation

The whole mechanism is implemented both in Python and in smart contracts where the directory contains the implementation of the AMMBA mechanism, designed for deployment on an Ethereum Virtual Machine (EVM)-compatible blockchain (e.g., Ethereum, Polygon). A personal Ethereum network can be simulated using Ganache or a Python environment (as in the context of this work). Ganache provides instant block mining and an HTTP interface for interaction.

The Truffle suite is used to write, compile, and deploy the smart contracts. This involves creating two standard ERC-20 contracts (EnergyToken and MoneyToken) and the main AMMBA contract. A migration script handles the deployment sequence: the token contracts are deployed first, and their resulting blockchain addresses are then used to initialize the AMMBA contract, linking them together. The OC-PF is also located in the smart contract to follow the sequence of market mechanism. The codebase implementation and the data are accessible on GitHub [63].

3.1.2. Double auction and uniform-price auction setups

To compare the performance of the AMMBA market with other mechanisms, DA and UPA market architectures are implemented as benchmark models. In this regard, at each time interval, market is cleared in which buyers and sellers submit their respective bids and offers. These bids and offers specify both the quantity of energy to be bought or sold and the corresponding price at which participants are willing to purchase or supply energy.

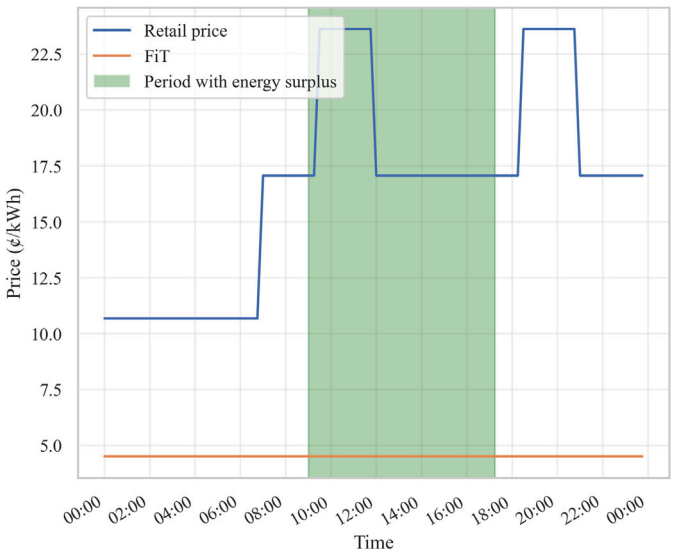

Fig. 5. Retail energy prices and FiT.

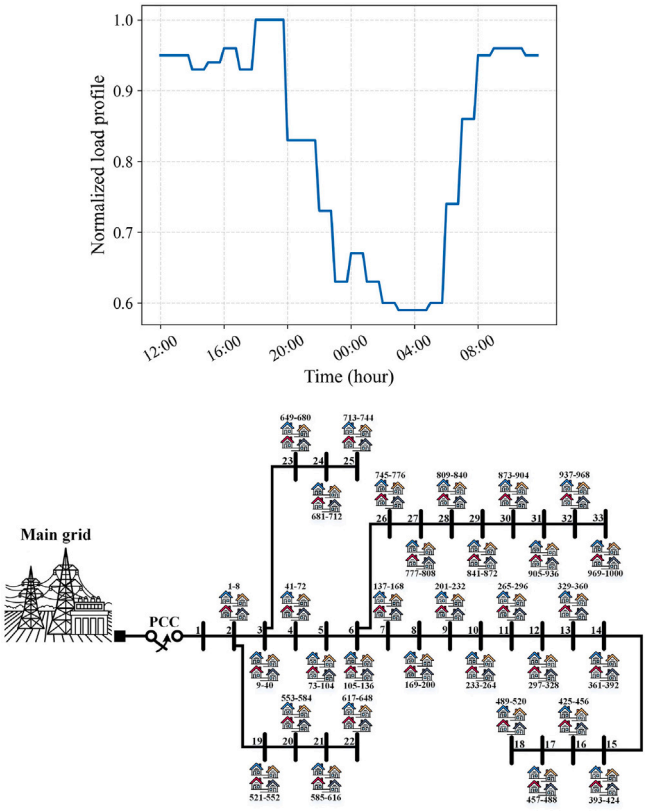

Fig. 6. Normalized load profile (top); Single-line diagram of the test system with 1000 households (bottom).

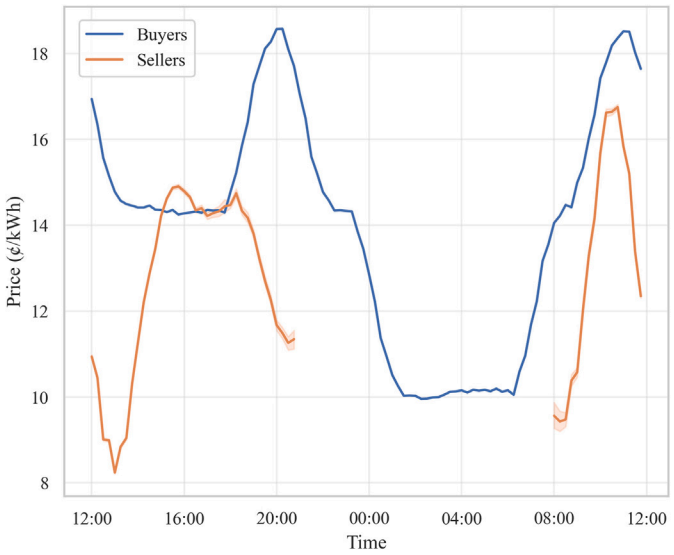

Fig. 7. Average bid and offer prices of traders for the high prosumer scenario.

As with the AMMBA simulation, households are assumed to have perfect foresight of their energy demand and production. The prices that buyers are willing to pay (i.e., the bid price) are randomly drawn from a normal distribution with mean $\mu = \frac{2}{3}K_{\mathrm{up},t}$ and standard deviation $\sigma = 0.01$. The same bid prices are used to determine the amount of deposited money for the AMMBA simulation. Conversely, the prices that sellers are willing to sell their surplus energy depend on the current retail price, the fixed FiT and the current amount of surplus energy S_T in relation to their peak surplus energy production $S_{\max}$. It is randomly drawn from a normal distribution with mean $\mu = \frac{0.75 S_T}{S_{\max}}\left(K_{\mathrm{up},t} + K_{\mathrm{lo}}\right)$ and standard deviation $\sigma = 0.03$. Fig. 7 shows the average bid and offer prices of buyer and seller agents during the high prosumer penetration scenario.

Given these bid and offer prices, the DA market then clears trades through a limit order book mechanism in a pay-as-bid pricing scheme. Buyers and sellers submit their orders in random sequence, and unmatched orders are stored in the order book—buy bids sorted from highest to lowest and sell offers from lowest to highest. A trade is executed whenever an incoming buy (sell) order meets a sell (buy) order at a compatible price, with the transaction price determined by the incoming order. If an order is only partially matched, the unfulfilled portion stays in the order book at the same price; fully matched orders are removed. At the end of each cycle, the order book is cleared of any remaining orders.

As a second benchmark, a UPA mechanism is also considered. In the UPA setup, buyers and sellers submit price-quantity pairs representing their willingness to buy or sell electricity. All buy bids are ranked in descending order of price, while sell offers are ranked in ascending order, forming the cumulative demand and supply curves, respectively. The market is cleared at the intersection of these curves, yielding a single uniform clearing price that applies to all accepted trades. Buyers with bid prices above the clearing price and sellers with offer prices below the clearing price participate in the transaction at this common price. The UPA mechanism is widely used in wholesale electricity markets and therefore serves as a meaningful benchmark for evaluating the performance of the proposed AMMBA mechanism.

3.2. Performance measures

There exist several evaluation indices in literature [64] that are used to benchmark P2P market mechanism performances.

The Value Tapping Index (VTI) measures how much of the theoretical cost-saving potential of P2P energy sharing is realized. It is calculated by comparing the total prosumer income and savings under the P2P mechanism ($value_{\mathrm{mec}}$) to the income in a non-P2P scenario ($value_{\mathrm{ref}}$) and the theoretical maximum ($value_{\max}$) achievable through perfect local energy sharing:

$$VTI = \frac{value_{\mathrm{mec}} - value_{\mathrm{ref}}}{value_{\max} - value_{\mathrm{ref}}} \tag{30}$$

The Participation Willingness Index (PWI) assesses the percentage of prosumers whose energy costs decrease under the P2P market. It is calculated as the ratio of prosumers with reduced costs (N_{rc}) to the total number of participants (N), reflecting the mechanism's attractiveness and inclusivity:

$$PWI = \frac{N_{\mathrm{rc}}}{N} \tag{31}$$

The Equality Index (EI) measures the fairness of income distribution among participants, based on a normalized Gini coefficient. It is derived from the Inequality Index (IEI), which calculates the relative mean absolute difference of incomes among all participants:

$$IEI = \frac{\sum_{n=1}^{N}\sum_{m=1}^{N}|Income'_n - Income'_m|}{2N\sum_{n=1}^{N} Income'_n} \tag{32}$$

The EI is then defined to be consistent with other indices, where a higher value is better as it indicates a more equal distribution of benefits:

$$EI = 1 - IEI \tag{33}$$

4. Simulation results and discussion

In this section, the results of the simulations carried out for the three scenarios with varying prosumer penetration in the community are analyzed. The results are compared to an equivalent market simulation based on a DA approach. Although both approaches are fundamentally different in their design, their price development, amounts of sold energy and induced welfare are comparable. It is worth mentioning that only the periods in which surplus energy production is available are simulated. For the AMMBA market simulations, the total amount of energy and money tokens deposited to the contract as well as the total amount of received money and energy tokens are recorded for each market participant at all times.

4.1. Parameter optimization results

Table 2 shows the results regarding the optimal midpoint and steepness parameters under all generation scenarios for $\alpha = 0.5$ and $\alpha = 0.4$. Across both α values, the steepness B decreases when α is reduced from 0.5 to 0.4, yielding flatter pricing curves and therefore more stable prices. Midpoint Θ also shifts downward with the lower α, but the relative ordering remains: scenarios with more installed generation capacity (moving from Low to High) require higher midpoints and lower steepness to preserve seller profitability while keeping the price trajectory responsive to the narrower range of energy-to-money ratios. For the subsequent market simulations we continue using $\alpha = 0.5$.

Table 2
Optimal midpoint and steepness parameters for different α.

Scenario	$\alpha = 0.5$		$\alpha = 0.4$	
	Θ	B	Θ	B
High	0.61	0.84	0.45	0.61
Medium	0.39	1.24	0.29	0.90
Low	0.25	2.51	0.16	1.74

Table 3
Aggregated KPIs of the AMMBA, UPA, and DA market simulations.

Scenario	Low	Medium	High
Demand and Surplus			
Total Demand	32,483 kWh	32,483 kWh	32,483 kWh
Total Surplus	7105 kWh	13,400 kWh	20,118 kWh
Market Metrics (AMMBA / UPA / DA)			
Total Profit (*e*)	278.3 / 554.9 / **292.8**	**445.6** / 694.8 / 362.9	**608.9** / 837.7 / 437.7
Utility (*e*)	**689.8** / 249.7 / 516.6	**916.8** / 429.1 / 764.7	**1058.5** / 534.2 / 939.2
Welfare (*e*)	**968** / 805 / 809	**1362** / 1124 / 1127	**1667** / 1372 / 1377
Indexes (AMMBA / UPA / DA)			
CSC (%)	**90.9** / 75.6 / 76.1	**67.2** / 54.7 / 55.0	**54.6** / 44.2 / 44.3
VTI (%)	**67.0** / 50.1 / 50.6	**55.7** / 38.2 / 38.5	**45.7** / 28.0 / 28.3
EI (%)	**39.4** / 33.4 / 36.7	**47.8** / **47.9** / 44.1	**54.7** / **56.4** / 49.8
PWI (%)	**100** / **97.6** / 89.4	**100** / 96.5 / 96.5	**100** / **100** / **100**

4.2. Markets analogy

In order to directly compare the market approaches, the aggregated KPIs that are calculated over all timesteps and households are compared (see Table 3). These include total supplier profit, total consumer utility, total welfare and community self-consumption (CSC). The CSC indicates how much of the total prosumers surplus energy production is traded and subsequently consumed by other members of the community. The VTI, PWI and EI are calculated as described in Section 3.2.

AMMBA trading consistently outperforms both the DA and UPA in terms of CSC. This is ultimately due to the fact that in both the DA and UPA, prosumers are not guaranteed to sell their energy surplus even when there is sufficient demand, whereas AMMBA always distributes all available energy supply to the consumers depending on their share of money deposits and the clearing price. Subsequently, the AMMBA market induces higher overall social welfare. As the prosumer-to-consumer ratio increases, the CSC of both the DA and UPA decreases. Notably, the UPA and DA produce nearly identical outcomes in CSC, VTI, and welfare across all scenarios, confirming that the performance gap is attributable to AMMBA's liquidity-pooling batch-auction design rather than to a particular weakness of competitive order matching.

The indexes reveal the core trade-off between the models. For the PWI, AMMBA achieves a perfect score (100%) in all scenarios, guaranteeing that every prosumer benefits. The UPA likewise achieves high PWI (97.6% in the Low scenario), because its uniform clearing price is more inclusive than the DA's discriminatory pricing; however, this advantage narrows as market liquidity grows. The larger welfare is reflected in the VTI which shows that cost savings and profits for prosumers are significantly higher with the AMMBA mechanism. The EI shows that AMMBA distributes the financial benefits more evenly among all participants. An interesting nuance is the profit-utility split: the UPA generates the highest seller profit of the three mechanisms but at the expense of substantially lower consumer utility. This is because the UPA clearing price is set by the marginal (highest accepted) offer, which tends to exceed the sigmoid-based AMMBA price that balances both sides by design. AMMBA's explicit optimization of the pricing function (Section 2.2) ensures a more equitable distribution of surplus between buyers and sellers.

To develop a better understanding of the benefits and weaknesses of both market approaches, the results are analyzed at the individual time frame level. Fig. 8 shows the development of the AMMBA uniform clearing price and the average trade price of the DA market across the three generation scenarios. The resulting clearing prices of the AMMBA market simulation over periods of available energy supply show that the prices are more stable at each timestep across the three scenarios, resulting from the higher liquidity.

While the average prices for energy in the simulated DA market follow a similar pattern to the uniform clearing prices of the AMMBA market, individual prices are significantly more volatile, as indicated by their standard deviation. In some cases, individual prices may reach the upper or lower price limit, resulting in a zero net utility/profit for the individual consumer or supplier household. This behavior becomes even more extreme as the prosumer-to-consumer ratio increases across generational scenarios.

Fig. 9 visualizes the total amount of energy traded at each time interval. In an optimal case, the amount of energy traded always corresponds to the amount of available energy surplus but since production exceeded demand, particularly in the medium and high prosumer scenarios, only the amount of energy up to the demand was sold. This figure shows that for the AMMBA simulation during all three scenarios under study, all energy demand is covered via P2P trading, thereby achieving superior self-consumption.

In the DA market, in some periods, some of the excess energy is not sold. This happens when suppliers offer their energy at a higher price than consumers are willing to pay, resulting in a lower CSC.

As explained in Section 2.2, the balance between consumer benefit and seller profit is critical to ensure that both sides achieve acceptable returns when trading in the market. For example, if the price always corresponds to the FiT rate during periods of high energy production, suppliers can simply sell the energy to their local energy company instead. Yet, if prices respond very little to changes in energy supply or demand, participants may perceive the market as highly regulated. More importantly, prices that reflect the current demand-to-supply ratio encourage consumers to adjust their demand to the current level of energy production, positively impacting the operation of the distribution grid [65]. The response of consumer demand to price changes is another highly relevant area in energy systems research but is out of scope for the simulated market environments in this work.

4.3. Performance evaluation of OC-PF

To evaluate the performance of the proposed on-chain distribution network modeling approach within the AMMBA energy trading framework, the high prosumer penetration scenario is considered. As a first step, the accuracy of the OC-PF formulation is evaluated against the full AC power flow model. In this regard, the nodal voltage magnitudes and line power flows obtained from the two power flow models are compared, and their deviations are illustrated in Fig. 10. As seen, the differences in voltage magnitude and line flow calculations between the OC-PF approximation and the full AC power flow solution are small, demonstrating the computational accuracy of the proposed formulation. Additionally, the amount of network losses is computed using the proposed OC-PF model and compared with the accurate losses obtained from the full AC power flow calculation. The average deviation between the two methods is approximately 2.5% over the daily simulation

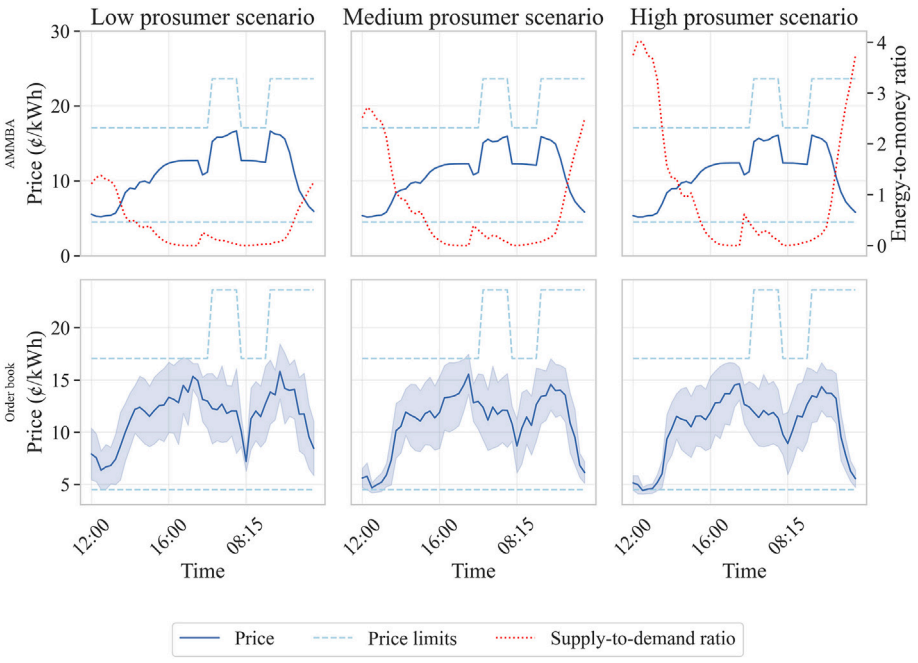

Fig. 8. Price development for different scenarios under AMMBA and DA.

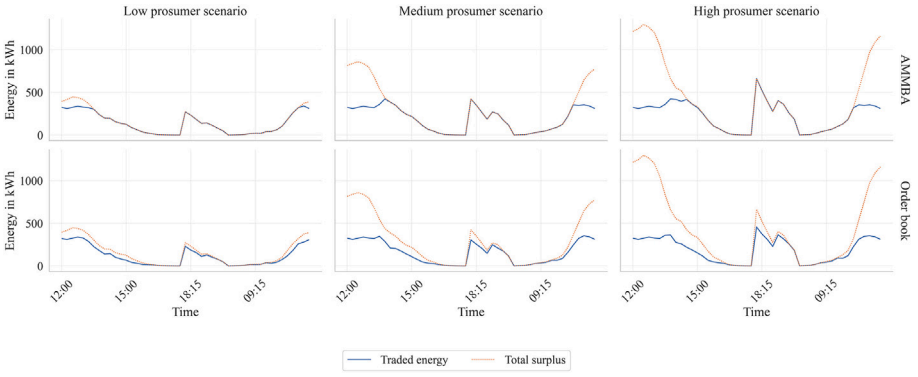

Fig. 9. Total sold energy.

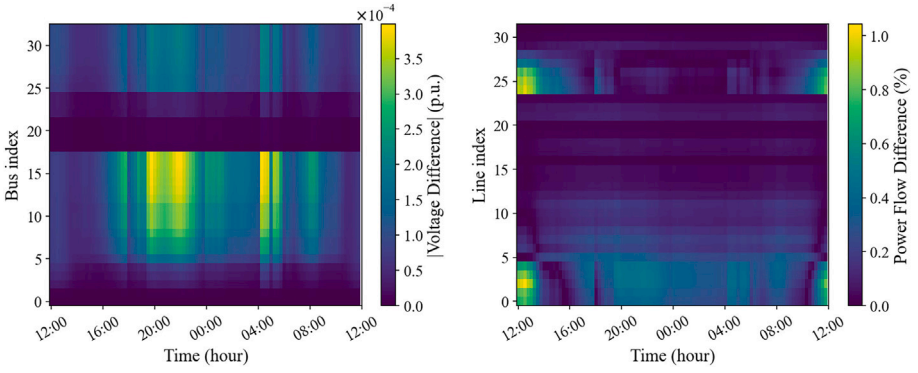

Fig. 10. Deviation between OC and AC power flow models: voltage error (left) and line flow error (right).

horizon. Overall, the proposed method demonstrates superior accuracy in power flow and network loss calculations compared to linearized power flow approaches such as piece-wise linear approximation, while preserving computational efficiency.

To assess network operational feasibility under household energy trading, the nodal voltage profiles are calculated using the proposed OC-PF model across all time intervals. The results indicate that voltage constraint violations occur at only two time intervals, i.e., 19:30 and

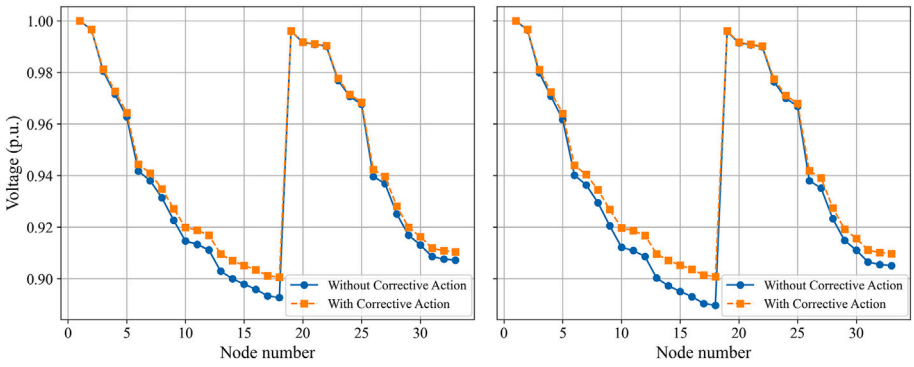

Fig. 11. Voltage profiles for time intervals with violations: 19:30 (left) and 19:45 (right).

Table 4
Impact of minimum voltage threshold on required adjustments.

V_{min} (p.u.)	Total adjustment (kWh)	No. of intervals with adjustment
0.88	0	0
0.89	1.69	1
0.90	102.56	2
0.91	988.79	23
0.92	3232.85	45

19:45, as illustrated by the corresponding voltage profiles in Fig. 11. To alleviate these voltage deviations, consumption adjustments were applied to the buyer agents, totaling 42.4 kWh for the 19:30 interval and 60.16 kWh for the 19:45 interval, which successfully restored the voltages at the violating nodes back within the allowable range.

To further assess the sensitivity of the corrective action mechanism under various voltage security requirements, the minimum allowable voltage threshold was varied across several values. For each case, the model was executed to determine both the total required adjustment and the number of intervals in which corrective action became necessary, with the numerical results summarized in Table 4. As expected, tightening the minimum voltage limit results in a greater number of intervals with voltage violations and accordingly increases the total adjustment needed to maintain voltages within the pre-defined acceptable range.

Moreover, although the original test network does not include any line flow constraints, active power flow limits are imposed on two representative lines—specifically, lines 2 (connecting nodes 2–3) and 26 (connecting nodes 26–27), with limits of 3600 kW and 900 kW, respectively—to demonstrate the capability of the proposed model in handling such constraints. Considering these limits, the active power flow profiles of both lines, before and after applying the corrective actions, are depicted in Fig. 12. The figure clearly shows that during peak hours, i.e., from 17:00 to 23:00, the highest line overloads occur, indicating that corrective actions are required during these intervals. To enforce the active power flow limits on these two lines, along with the previously mentioned voltage constraint, the total consumption of buyer agents is reduced by 1494.62 kWh over all time intervals. This consumption adjustment results in decreases of 1685.27 kWh and 450.30 kWh in the electricity flows through lines 2 and 26, respectively, as shown by the shaded regions in the figure, effectively bringing the power flows of these lines back within specified limits.

After determining the exchanged energy for all market participants while accounting for network security constraints, the resulting network losses are computed. As discussed earlier, these losses are allocated fairly among participants based on their contributions using the concept of marginal loss factors. To illustrate this, Fig. 13 shows the average losses for each relevant household in loss allocation over a 24-hour period, along with the distribution of allocated losses among households during the same period. As seen in the figure, during the periods between approximately 10:00 and 14:00, when there is surplus generation, the network losses resulting from energy trading are negative, creating a benefit that is fairly allocated to the seller agents. Conversely, during the remaining time intervals, the network losses are positive, and the corresponding additional cost is fairly distributed among the buyer agents. It is worth mentioning that the marginal loss factor values are positive for all nodes across all time intervals; therefore, in periods of negative losses, the relevant agents are the sellers, while in periods of positive losses, the relevant agents are the buyers.

To illustrate the impact of allocated network losses on the final energy trading price for each market participant, Fig. 14 shows the uniform AMMBA clearing prices for each time interval alongside the distribution of the final energy trading prices after considering loss allocation. The

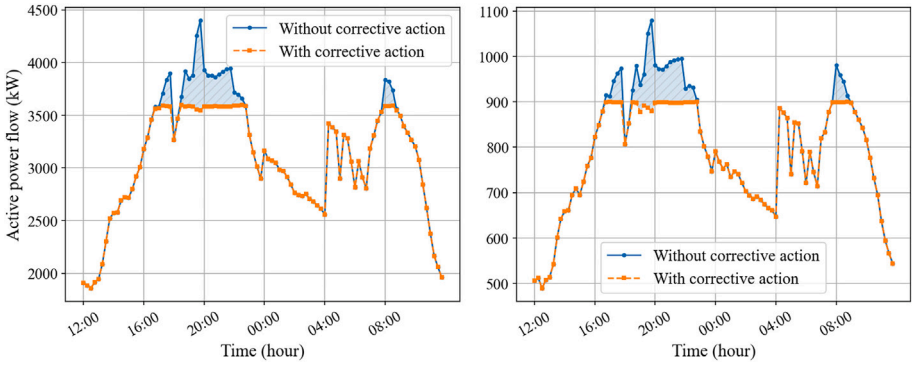

Fig. 12. Active power flow on line 2 (left) and line 26 (right).

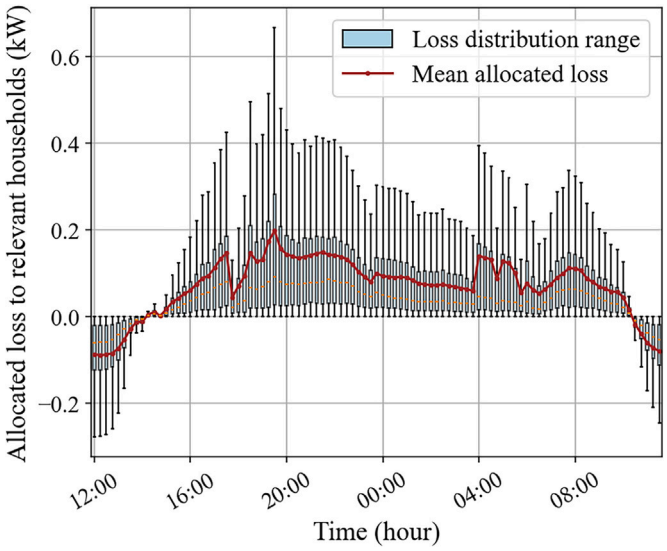

Fig. 13. Allocated losses among the relevant market participants.

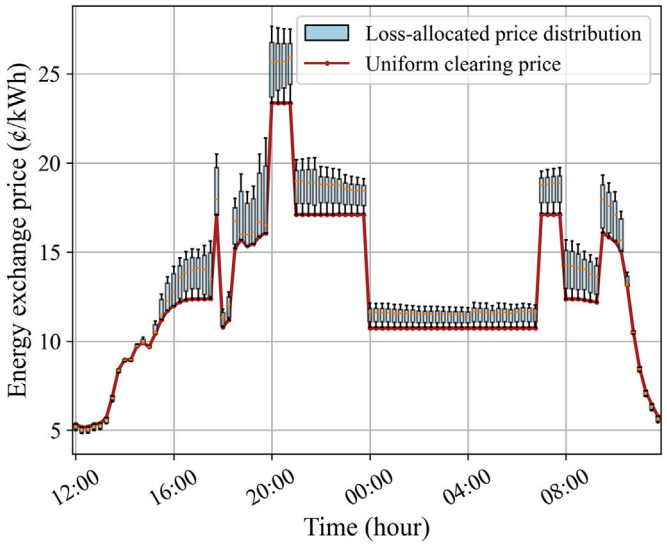

Fig. 14. Clearing price and loss-allocated final price for market participants.

figure shows how the proposed loss allocation method adjusts the effective price for each participant based on their contribution to network losses, introducing variability around the uniform clearing price while maintaining a fair and transparent settlement mechanism.

4.4. Sensitivity analysis

To further evaluate the robustness of the proposed AMMBA mechanism under informational uncertainty, a sensitivity analysis is conducted. In the simulation study, perfect foresight of household demand and surplus is initially assumed within each 15-minute settlement cycle. However, in practical settings, short-term forecast errors may affect reported consumption and generation values. To examine the impact of prediction uncertainty, zero-mean Gaussian noise is introduced to the demand and surplus reports, with the noise standard deviation σ varying from 0% to 20% of the true value. Table 5 presents the performance of the proposed mechanism under different levels of forecast error.

This table shows that the key performance metrics of AMMBA - including CSC, VTI, and total social welfare - remain relatively stable,

Table 5
AMMBA robustness to demand/supply forecast errors (high scenario, $\bar{\Delta}$ over 5 realisations).

Forecast error σ	CSC (Δ)	VTI (Δ)	PWI	EI	Welfare (Δ)
0%	0.546 (+0.0%)	0.457 (−0.0%)	0.511	0.547	1667.42 (+0.0%)
5%	0.546 (+0.0%)	0.457 (+0.0%)	0.507	0.547	1668.10 (+0.0%)
10%	0.546 (+0.1%)	0.457 (+0.1%)	0.510	0.547	1668.79 (+0.1%)
15%	0.547 (+0.1%)	0.458 (+0.1%)	0.510	0.547	1669.48 (+0.1%)
20%	0.547 (+0.1%)	0.458 (+0.2%)	0.510	0.546	1670.17 (+0.2%)

σ = noise standard deviation as fraction of true value. Values in parentheses show percentage change relative to the perfect-foresight baseline ($\sigma = 0$). Metrics are averaged over 5 independent noise realisations. AMMBA parameters are optimized on clean (perfect-foresight) training data throughout.

with variations below 0.2% even at $\sigma = 20\%$. This indicates that the proposed batch auction structure provides inherent robustness to moderate informational uncertainty, since the clearing price is determined by the aggregate supply-to-demand ratio rather than individual reports, allowing local forecast errors to partially offset at the community level.

5. Conclusions and future works

This study proposed an AMMBA mechanism, a novel energy market design inspired by DeFi principles to address the liquidity and volatility challenges in local, P2P energy trading markets. By incorporating shortfall and externality penalties, the mechanism preserves participation incentives and supports the long-term sustainability of the community energy market by maintaining economic balance and profitability for prosumers as renewable energy penetration increases. The framework integrated an OC-PF model to address network constraint violations arising from energy trading, along with an ex-post MLF-based loss-allocation mechanism that fairly reflects participants' contributions to network losses in their energy trading prices.

Through a comprehensive simulation study, the numerical results provide quantitative evidence of the advantages of the proposed model when benchmarked against two traditional mechanisms, i.e., DA and UPA. The findings demonstrate that AMMBA offers superior performance across several key metrics. Specifically, the proposed AMMBA mechanism achieves superior CSC across all scenarios, increasing CSC by approximately 20% on average compared with the benchmark DA and UPA mechanisms. The improved utilization of locally generated energy contributes to higher overall social welfare and enhanced financial performance of the community, as reflected in the VTI. Furthermore, AMMBA ensures broader and more equitable market participation, achieving a PWI of 100%, indicating that no participant experiences financial disadvantage. The model also demonstrates strong fairness performance in terms of EI, reflecting a balanced distribution of economic benefits among market participants. These outcomes stem from a mechanism design that prioritizes guaranteed allocation and price stability over the limitations of conventional DA and UPA mechanisms under low-liquidity conditions. Through dynamic parameter optimization of the sigmoid pricing function, this study demonstrates that by optimal fine-tuning of price function parameters, the AMMBA can adapt to different prosumer-to-consumer ratios. Additionally, the numerical results demonstrate that the proposed P2P energy trading model enforces network security constraints while requiring only minimal consumption or generation adjustments from market participants and fairly allocating network losses according to their actual contributions.

Our analysis relied on two simplifying assumptions. First, we assumed perfect foresight of consumption and production within each settlement cycle. Sensitivity analysis indicates that the AMMBA mechanism is robust to realistic forecast inaccuracies, due to its batch-auction design that aggregates supply and demand. Second, long-term behavioral dynamics, such as evolving participant strategies, were not considered;

incorporating such dynamics in future work could provide further insights into how different market designs incentivize grid-supportive actions over time.

Several avenues for future research emerge from this work. From a data governance perspective, on-chain privacy remains a key challenge, as storing granular household consumption and generation data on a public immutable ledger may conflict with data protection regulations. While private or permissioned blockchains provide a basic mitigation, future work should focus on advanced cryptographic and architectural solutions. In particular, Zero-Knowledge Proof (ZKP) schemes could enable smart contracts to verify transaction validity and penalty compliance without exposing sensitive user data, while hybrid architectures combining off-chain encrypted storage with on-chain verification may offer a balanced trade-off between transparency, auditability, and regulatory compliance. Beyond privacy considerations, further research is needed to strengthen the mechanism's robustness against strategic coordination. Although the current incentive-compatibility analysis addresses individual rational behavior, extending the penalty framework toward coalition-proof market designs capable of deterring coordinated supply withholding by groups of prosumers represents an important theoretical advancement. Finally, real-world pilot demonstrations with active participation from community members constitute a critical next step. Empirical deployment would allow the validation of behavioral responses to the pricing and penalty structure, the assessment of user acceptance, and the refinement of governance models, thereby ensuring that the proposed market framework remains technically sound, economically viable, and socially accepted in practical implementations.

CRediT authorship contribution statement

Hossein Saber: Writing – review & editing, Writing – original draft, Visualization, Software, Methodology, Investigation, Formal analysis, Data curation. **Tom Celig:** Writing – review & editing, Writing – original draft, Visualization, Validation, Software, Methodology, Investigation, Formal analysis, Data curation, Conceptualization. **Saber Talari:** Writing – review & editing, Writing – original draft, Visualization, Validation, Supervision, Software, Resources, Project administration, Methodology, Investigation, Formal analysis, Data curation, Conceptualization. **Wolfgang Ketter:** Writing – review & editing, Validation, Supervision, Project administration. **Detlef Schoder:** Writing – review & editing, Validation, Supervision, Resources, Project administration.

Declaration of competing interest

The authors declare that they have no known competing financial interests or personal relationships that could have appeared to influence the work reported in this paper.

Acknowledgment

This work was supported by EU's Horizon Europe research and innovation programme under grant agreement N° 101160678 (Project: INTELLIGENT).

Appendix A. Detailed rule-based scheduling logic

A.1. PV scheduling

PV generation is treated as a priority energy source. At each time interval, the PV output is first allocated to meet the household's demand. Any remaining surplus is then allocated based on the priorities of the household assets and may be used to charge the battery or the EV, or be offered for trading with other prosumers or consumers through the AMMBA mechanism. As a result, all available PV generation is fully utilized without curtailment.

A.2. Battery scheduling

The battery operates according to price-driven rule-based logic that incorporates electricity prices, degradation costs, and technical constraints. At each time interval, the battery evaluates the forecasted clearing price and determines whether charging, discharging, or remaining idle leads to the highest economic benefit. Specifically, charging occurs when the current price falls below a predefined lower threshold and the expected price increase over the look-ahead horizon $[t, t+H]$ is large enough to compensate for both the battery degradation cost and round-trip efficiency losses. Thus, the battery charges at time t if:

$$\pi_t^f < \pi^{\text{low}} \quad \text{and} \quad \max(\pi_{t:t+H}^f) - \pi_t^f > \frac{C^{\text{deg}}}{\eta^{\text{rt}}} \tag{A.1}$$

where π_t^f is the forecasted clearing price at time t, π^{low} is a predefined lower threshold, H is the look-ahead horizon, C^{deg} is the degradation price of battery, and η^{rt} is the round-trip efficiency. The amount of charging power is restricted by both its rated power ($P^{\text{ch,r}}$) and the maximum allowable state of energy ($SOE^{\max}$):

$$P_t^{\text{ch}} = \min\left(P^{\text{ch,r}}, \frac{SOE^{\max} - SOE_t}{\eta^{\text{ch}}\tau}\right) \tag{A.2}$$

In the above, SOE_t, η^{ch}, and τ denote the current SOE level, the charging efficiency, and the duration of time interval (e.g., 15 minutes), respectively. Conversely, discharging takes place when the current price exceeds an upper threshold and the expected price drop during the look-ahead horizon is sufficiently large, i.e., when

$$\pi_t^f > \pi^{\text{high}} \quad \text{and} \quad \pi_t^f - \min(\pi_{t:t+H}^f) > \frac{C^{\text{deg}}}{\eta^{\text{rt}}} \tag{A.3}$$

where π^{high} is a predefined upper threshold. The amount of discharging power is restricted by both its rated power ($P^{\text{dch,r}}$) and the minimum allowable state of energy ($SOE^{\min}$):

$$P_t^{\text{dch}} = \min\left(P^{\text{dch,r}}, \frac{(SOE_t - SOE^{\min})\eta^{\text{dch}}}{\tau}\right) \tag{A.4}$$

where η^{dch} denotes the discharging efficiency. Finally, if neither of the conditions for charging (A.1) nor discharging (A.3) are satisfied, the battery remains idle and does not charge or discharge.

A.3. EV charging

The EV charging process is managed based on the available plugged-in time and the required energy to reach the desired SOE by the scheduled departure time. The required charging duration to achieve the target SOE, as well as the available plugged-in time, are calculated as follows as stated by Saber et al. [66].

$$t^r = \frac{SOE^{\text{EV,des}} - SOE_t^{\text{EV}}}{\eta^{\text{EV,ch}}\, P^{\text{EV,r}}} \tag{A.5}$$

$$t^a = DT - CT \tag{A.6}$$

where $SOE^{\text{EV,des}}$ and SOE_t^{EV} denote the desired SOE at departure and the current SOE of the EV battery, $\eta^{\text{EV,ch}}$ and $P^{\text{EV,r}}$ are the charging efficiency and rated charging power of the EV battery, and DT and CT represent the departure and the current time intervals.

If the required charging time exceeds the available plugged-in time ($t^r \geq t^a$), the EV charges continuously at rated power by the scheduled departure time, acting as a non-flexible load. Conversely, if the required charging time is less than the available plugged-in time ($t^r < t^a$), the EV charges flexibly according to the forecasted electricity prices. In this case, charging occurs only when the forecasted price is below a price threshold. In our approach, this threshold is calculated individually for

each vehicle based on the ratio of required charging time to plugged-in time upon arrival. Specifically, the percentile of forecasted prices during the vehicle's connected period corresponding to this ratio is used as the threshold. For example, if t^r is very close to t^a, the ratio approaches one, resulting in a high percentile and thus a high price threshold. This ensures that the EV charges almost continuously, even at relatively high prices, to meet the desired state of charge. Conversely, if t^r is much smaller than t^a, the ratio is low, yielding a lower percentile and a lower price threshold. In this case, the EV charges only during the lowest-price intervals, exploiting price flexibility and minimizing electricity costs. The EV's charging power is then determined as follows as described by Saber et al. [67].

$$P_t^{\mathrm{EV}} = \min\left(P^{\mathrm{EV,r}}, \frac{SOE^{\mathrm{EV,des}} - SOE_t^{\mathrm{EV}}}{\eta^{\mathrm{EV,ch}}\tau}\right) \tag{A.7}$$

Appendix B. Voltage magnitude calculation using the OC-PF model

B.1. Definition of virtual variables for the OC-PF model

The active power loss of feeder nm in an AC power flow formulation can be calculated as the sum of the power flows in both directions, from node n to node m and vice versa, as follows.

$$P_{nm} = \frac{R_{nm}V_n^2 - R_{nm}V_nV_m\cos\delta_{nm} + X_{nm}V_nV_m\sin\delta_{nm}}{R_{nm}^2 + X_{nm}^2} \tag{B.1}$$

$$P_{mn} = \frac{R_{nm}V_m^2 - R_{nm}V_mV_n\cos\delta_{nm} - X_{nm}V_mV_n\sin\delta_{nm}}{R_{nm}^2 + X_{nm}^2} \tag{B.2}$$

$$P_{nm}^{loss} = P_{nm} + P_{mn} = \frac{R_{nm}\left(V_n^2 + V_m^2 - 2V_nV_m\cos\delta_{nm}\right)}{R_{nm}^2 + X_{nm}^2} \tag{B.3}$$

where P_{nm} and P_{mn} denote the active power flows in both directions of feeder nm, R_{nm} and X_{nm} represent its resistance and reactance, and V_n, V_m, and δ_{nm} denote the voltage magnitudes at nodes n and m and their voltage angle difference, respectively. By defining the virtual variables as $P_{nm}^* = P_{nm}/V_n$ and $P_{mn}^* = P_{mn}/V_m$, and assuming $\delta_{nm} \approx 0$ (due to the short distance between successive nodes), the feeder loss term can be expressed as:

$$P_{nm}^{loss*} \xrightarrow{\delta_{nm}\approx 0} \frac{R_{nm}\left(V_n + V_m - V_m - V_n\right)}{R_{nm}^2 + X_{nm}^2} = 0 \tag{B.4}$$

Thus, in the space of virtual variables introduced above, feeder losses vanish, and the power flowing through each feeder can be expressed as a linear function of the nodal power injections.

B.2. Voltage magnitude calculation using the OC-PF model

Assuming the virtual variables associated with the resistance and reactance of feeders in the OC-PF model are defined as

$$R_{nm}^* = \frac{R_{nm}}{R_{nm}^2 + X_{nm}^2}, \tag{B.5}$$

$$X_{nm}^* = \frac{X_{nm}}{R_{nm}^2 + X_{nm}^2}, \tag{B.6}$$

and taking Eq. (B.1) into account, the following relations can be derived for the line connecting nodes n and m:

$$R_{nm}^*P_{nm}^* = \left(R_{nm}^*\right)^2(V_n - V_m) + R_{nm}^*X_{nm}^*V_m(\delta_n - \delta_m) \tag{B.7}$$

$$X_{nm}^*Q_{nm}^* = \left(X_{nm}^*\right)^2(V_n - V_m) - R_{nm}^*X_{nm}^*V_m(\delta_n - \delta_m) \tag{B.8}$$

By combining the above two equations, we have:

$$V_n - V_m = \frac{R_{nm}^*}{\left(R_{nm}^*\right)^2 + \left(X_{nm}^*\right)^2}P_{nm}^* + \frac{X_{nm}^*}{\left(R_{nm}^*\right)^2 + \left(X_{nm}^*\right)^2}Q_{nm}^*$$

By substituting the virtual variables R_{nm}^* and X_{nm}^* from (B.5) and (B.6) into the above relations, the voltage difference between successive nodes can be expressed in the simplified form:

$$V_n - V_m = R_{nm}P_{nm}^* + X_{nm}Q_{nm}^*$$

Extending this formulation along a path from node 1 to node m, the voltage difference can be expressed as:

$$V_m - V_1 = -\sum_{nm\in\mathrm{Path}(1:m)} R_{nm}P_{nm}^* - \sum_{nm\in\mathrm{Path}(1:m)} X_{nm}Q_{nm}^*$$

Finally, the above equation can be further expressed in matrix form as:

$$\mathbf{V} = \mathbf{V}_1 - \mathbf{H}_v(\mathbf{r}\odot\mathbf{F}^{p,*}) - \mathbf{H}_v(\mathbf{x}\odot\mathbf{F}^{q,*}) \tag{B.9}$$

Appendix C. Decentralized solution via lagrangian relaxation

The optimization problem formulated for corrective actions, i.e., (15)–(18), is solved in a decentralized manner using the Lagrangian Relaxation (LR) method. The coupling constraints on branch flows and node voltages, which link multiple agents through the sensitivity matrices, are relaxed by introducing Lagrange multipliers (dual variables) $\bar{\lambda}$ and $\underline{\lambda}$ for the upper and lower branch flow limits, and $\bar{\mu}$ and $\underline{\mu}$ for the voltage limits. The resulting Lagrangian function is expressed in matrix form as:

$$\begin{aligned}\mathcal{L}(\Delta\mathbf{P},\bar{\lambda},\underline{\lambda},\bar{\mu},\underline{\mu}) = {}& \Delta\mathbf{P}^\top\Delta\mathbf{P} + (\bar{\lambda})^\top\left(\mathbf{S}_f\Delta\mathbf{P} - (\mathbf{F}^p_{\mathrm{AMMBA}} - \mathbf{F}^p_{\min})\right)\\ &+ (\underline{\lambda})^\top\left((\mathbf{F}^p_{\mathrm{AMMBA}} - \mathbf{F}^p_{\max}) - \mathbf{S}_f\Delta\mathbf{P}\right)\\ &+ (\bar{\mu})^\top\left(\mathbf{S}_v\Delta\mathbf{P} - (\mathbf{V}_{\max} - \mathbf{V}_{\mathrm{AMMBA}})\right)\\ &+ (\underline{\mu})^\top\left((\mathbf{V}_{\min} - \mathbf{V}_{\mathrm{AMMBA}}) - \mathbf{S}_v\Delta\mathbf{P}\right)\end{aligned} \tag{C.1}$$

Due to the separability of the objective and linearity of the constraints, the problem decomposes into independent subproblems for each agent a, where the agent minimizes

$$\min_{\Delta P_a} \quad \Delta P_a^2 + \Delta P_a\phi_a, \quad \text{s.t.} \quad \mathbf{P}_{\min,a} \le \Delta P_a \le \mathbf{P}_{\max,a} \tag{C.2}$$

with

$$\phi_a = \mathbf{S}_{f_{:,a}}^\top(\bar{\lambda} - \underline{\lambda}) + \mathbf{S}_{v_{:,a}}^\top(\bar{\mu} - \underline{\mu}) \tag{C.3}$$

where $\mathbf{S}_{f_{:,a}}$ and $\mathbf{S}_{v_{:,a}}$ denote the a-th column of the corresponding sensitivity matrices. Finally, the closed-form solution of the subproblem for each agent is formulated as (21) and (22).

The system operator (master) collects the agents' solutions and updates the Lagrangian multipliers using a subgradient method:

$$\bar{\lambda}^{(k+1)} = \left[\bar{\lambda}^{(k)} + \alpha_k(\mathbf{S}_f\Delta\mathbf{P} - (\mathbf{F}^p_{\mathrm{AMMBA}} - \mathbf{F}^p_{\min}))\right]^+ \tag{C.4}$$

$$\underline{\lambda}^{(k+1)} = \left[\underline{\lambda}^{(k)} + \alpha_k((\mathbf{F}^p_{\mathrm{AMMBA}} - \mathbf{F}^p_{\max}) - \mathbf{S}_f\Delta\mathbf{P})\right]^+ \tag{C.5}$$

$$\bar{\mu}^{(k+1)} = \left[\bar{\mu}^{(k)} + \alpha_k(\mathbf{S}_v\Delta\mathbf{P} - (\mathbf{V}_{\max} - \mathbf{V}_{\mathrm{AMMBA}}))\right]^+ \tag{C.6}$$

$$\underline{\mu}^{(k+1)} = \left[\underline{\mu}^{(k)} + \alpha_k((\mathbf{V}_{\min} - \mathbf{V}_{\mathrm{AMMBA}}) - \mathbf{S}_v\Delta\mathbf{P})\right]^+ \tag{C.7}$$

where α_k is a positive step size, and $[\cdot]^+$ denotes the projection onto the non-negative orthant. This decentralized iterative procedure continues until the convergence criterion is met, that is, when the Euclidean norms of the differences of both the primal variables ($\Delta\mathbf{P}$) and the dual variables (λ and μ) between successive iterations fall below predefined thresholds.

Appendix D. Loss allocation

D.1. Derivation of network loss formula

The total power loss in the network is defined as the sum of the power flows on all feeders and can be written as

$$P^{\text{loss}} = \sum_{n=1}^{N_B} \left(P_{nm} + P_{mn} \right) \tag{D.1}$$

where P_{nm} and P_{mn} are the flowing power through the feeder connecting nodes n and m. Using the virtual power flow variables of the OC-PF model ($P_{nm} = V_n P^*_{nm}$ and $P_{mn} = V_m P^*_{mn}$), the above expression can be rewritten as

$$P^{\text{loss}} = \sum_{n=1}^{N_B} \left(V_n P^*_{nm} + V_m P^*_{mn} \right) \overset{P^*_{nm} = -P^*_{mn}}{=} \sum_{n=1}^{N_B} \left(V_n - V_m \right) P^*_{nm} \tag{D.2}$$

Expressing the virtual feeder flows P^*_{nm} in terms of the virtual nodal consumptions of the downstream nodes and telescoping along the path from the node 1 to each node n gives

$$P^{\text{loss}} = \sum_{n=1}^{N_B} \left(V_1 - V_n \right) P^*_n \tag{D.3}$$

with $V_1 = 1$ p.u. and using the relation $P^*_n = P_n / V_n$, we finally obtain the network power losses as follows.

$$P^{\text{loss}} = \sum_{n=1}^{N_B} \left(P^*_n - P_n \right) = \sum_{n=1}^{N_B} P_n \left(\frac{1}{V_n} - 1 \right) \tag{D.4}$$

D.2. Derivation of MLF formula

The MLF value for node m, which quantifies the impact of an incremental change in power withdrawal at that node on the total network losses, is computed as:

$$\gamma_m = \frac{\partial P^{\text{loss}}}{\partial P_m} = \frac{\partial}{\partial P_m} \sum_{n=1}^{N_B} P_n \left(\frac{1}{V_n} - 1 \right) = \left(\frac{1}{V_m} - 1 \right) + \sum_{n=1}^{N_B} P_n \left(\frac{-V'_n}{V_n^2} \right) \tag{D.5}$$

To calculate $V'_n = \partial V_n / \partial P_m$, we use the OC-PF model (14), defining $\mathrm{C} = \mathrm{H}_v(\mathrm{r} \odot_{\mathrm{c}} \mathrm{A}_f)$ and $\mathrm{E} = \mathrm{H}_v(\mathrm{x} \odot_{\mathrm{c}} \mathrm{A}_f)$. With these definitions, the voltage magnitudes can be expressed as follows.

$$\mathbf{V} = \mathbf{V}_1 - \mathbf{C}(\mathbf{P} \oslash \mathbf{V}) - \mathbf{E}(\mathbf{Q} \oslash \mathbf{V}) \tag{D.6}$$

and equivalently, for each node n, as:

$$V_n = V_{1n} - \sum_{k=1}^{N_B} \frac{C_{nk}}{V_k} P_k - \sum_{k=1}^{N_B} \frac{E_{nk}}{V_k} Q_k \tag{D.7}$$

Taking the partial derivative of V_n with respect to P_m yields:

$$\frac{\partial V_n}{\partial P_m} = \sum_{k=1}^{N_B} \frac{C_{nk}}{V_k^2} \frac{\partial V_k}{\partial P_m} P_k - \frac{C_{nm}}{V_m} + \sum_{k=1}^{N_B} \frac{E_{nk}}{V_k^2} \frac{\partial V_k}{\partial P_m} Q_k \tag{D.8}$$

By defining the sensitivity matrix $\mathbf{D}$ with entries $D_{nm} = \partial V_n / \partial P_m$, we obtain:

$$D_{nm} = \sum_{k=1}^{N_B} (C_{nk} \frac{P_k}{V_k^2} D_{km} + E_{nk} \frac{Q_k}{V_k^2} D_{km}) - \frac{C_{nm}}{V_m} \tag{D.9}$$

This recursive expression can be reformulated in matrix form as:

$$\mathbf{D} = \left(\mathbf{C} \odot_{\mathrm{r}} (\mathbf{P} \oslash \mathbf{V}^{\odot 2}) + \mathbf{E} \odot_{\mathrm{r}} (\mathbf{Q} \oslash \mathbf{V}^{\odot 2}) \right) \mathbf{D} - \mathbf{C} \oslash_{\mathrm{r}} \mathbf{V} \tag{D.10}$$

$$\left(\mathbf{I} - \mathbf{C} \odot_{\mathrm{r}} (\mathbf{P} \oslash \mathbf{V}^{\odot 2}) + \mathbf{E} \odot_{\mathrm{r}} (\mathbf{Q} \oslash \mathbf{V}^{\odot 2}) \right) \mathbf{D} = -\mathbf{C} \oslash_{\mathrm{r}} \mathbf{V} \tag{D.11}$$

$$\mathbf{D} = \left(\mathbf{I} - \mathbf{C} \odot_{\mathrm{r}} (\mathbf{P} \oslash \mathbf{V}^{\odot 2}) + \mathbf{E} \odot_{\mathrm{r}} (\mathbf{Q} \oslash \mathbf{V}^{\odot 2}) \right)^{-1} \left(- \mathbf{C} \oslash_{\mathrm{r}} \mathbf{V} \right) \tag{D.12}$$

Finally, using (D.5), the MLF vector ($\mathbf{\Gamma}$) is obtained as follows.

$$\mathbf{\Gamma} = (\mathbf{1} \oslash \mathbf{V} - \mathbf{1}) - \mathbf{D} \left(\mathbf{P} \oslash \mathbf{V}^{\odot 2} \right) \tag{D.13}$$

Eq. (D.13) represents the closed-form relation for computing the nodal marginal loss factors, which are then used in the main text to allocate the costs or benefits of network losses caused by the AMMBA energy exchanges among market participants.

Data availability

The GitHub repository for the code and data is cited in the manuscript.

References

[1] European Commission. REPowerEU plan: accelerating the green energy transition, 2024, https://energy.ec.europa.eu/topics/energy-strategy/repowereu_en [Accessed 10 November 2025].

[2] Solar Power Europe. Global market outlook for solar power 2025-2029: focus on India, 2025. https://api.solarpowereurope.org/uploads/Global_Market_Outlook_2025_v1_aaebd9698b.pdf?updated_at=2025-05-05T08:46:30.243Z [Accessed 29 October 2025].

[3] Abdolahinia H, Saber H, Parvini Z, Moeini-Aghtaie M. Developing a peer-to-peer energy trading model for battery storage considering carbon emission permission. Electr Power Syst Res 2024;237:111003.

[4] European Parliament and Council. Directive (EU) 2019/944 on common rules for the internal market for electricity and amending directive 2012/27/eu, 2019, https://eur-lex.europa.eu/legal-content/EN/TXT/?uri=CELEX [Accessed 10 November 2025].

[5] Caramizaru A, Uihlein A. Energy communities: an overview of energy and social innovation. Tech. Rep. JRC119433Accessed, European Commission, Joint Research Centre (JRC); 2020. https://doi.org/10.2760/180576. https://publications.jrc.ec.europa.eu/repository/handle/JRC119433 [Accessed 10 November 2025].

[6] Ketter W, Collins J, Reddy P. Power TAC: a competitive economic simulation of the smart grid. Energy Econ 2013;39:262–70.

[7] Hassan A, El-Amin I. Formulation of billing policy for residential scale solar PV systems and its impact in the kingdom of Saudi Arabia. Renew Energy Focus 2024;49:100568.

[8] Statistics | Eurostat Oct, 2024. https://ec.europa.eu/eurostat/databrowser/view/nrg_pc_204/default/table?lang=en.

[9] Aktuelle einspeisevergütung für PV-anlagen in 2024/2025 Dec, 2024. https://www.enpal.de/photovoltaik/einspeiseverguetung.

[10] Wang Z, Luther M, Horan P, Matthews J, Liu C. Technical and economic analyses of grid-connected residential PV considering batteries and peer-to-peer energy sharing. Renew Energy 2025:123494.

[11] Chiarini A, Compagnucci L. Blockchain, data protection and P2P energy trading: a review on legal and economic challenges. Sustainability 2022;14(23):16305.

[12] Shahidehpour M, Yan M, Shikhar P, Bahramirad S, Paaso A. Blockchain for peer-to-peer transactive energy trading in networked microgrids: providing an effective and decentralized strategy. IEEE Electrif Mag 2020;8(4):80–90.

[13] Liu Y, Li Z, Huang L. The application of blockchain technology in smart sustainable energy business model. Energy Rep 2022;8:7063–70.

[14] Paudel A, Chaudhari K, Long C, Gooi HB. Peer-to-peer energy trading in a prosumer-based community microgrid: a game-theoretic model. IEEE Trans Ind Electron 2018;66(8):6087–97.

[15] Troncia M, Galici M, Mureddu M, Ghiani E, Pilo F. Distributed ledger technologies for peer-to-peer local markets in distribution networks. Energies 2019;12(17):3249.

[16] Talari S, Khorasany M, Razzaghi R, Ketter W, Gazafroudi AS. Mechanism design for decentralized peer-to-peer energy trading considering heterogeneous preferences. Sustain Cities Soc 2022;87:104182.

[17] Wang Z, Yu X, Mu Y, Jia H. A distributed peer-to-peer energy transaction method for diversified prosumers in urban community microgrid system. Appl Energy 2020;260:114327.

[18] Li Z, Shahidehpour M, Alabdulwahab A, Al-Turki Y. Valuation of distributed energy resources in active distribution networks. Electr J 2019;32(4):27–36.

[19] Lyu X, Xu Z, Wang N, Fu M, Xu W. A two-layer interactive mechanism for peer-to-peer energy trading among virtual power plants. Energies 2019;12(19):3628.

[20] Sorin E, Bobo L, Pinson P. Consensus-based approach to peer-to-peer electricity markets with product differentiation. IEEE Trans Power Syst 2018;34(2):994–1004.

[21] Khorasany M, Gazafroudi AS, Razzaghi R, Morstyn T, Shafie-Khah M. A framework for participation of prosumers in peer-to-peer energy trading and flexibility markets. Appl Energy 2022;314:118907.

[22] AlSkaif T, Crespo-Vazquez JL, Sekuloski M, Van Leeuwen G, Catalão JPS. Blockchain-based fully peer-to-peer energy trading strategies for residential energy systems. IEEE Trans Ind Inform 2021;18(1):231–41.

[23] Abdella J, Tari Z, Anwar A, Mahmood A, Han F. An architecture and performance evaluation of blockchain-based peer-to-peer energy trading. IEEE Trans Smart Grid 2021;12(4):3364–78.

[24] Doan HT, Cho J, Kim D. Peer-to-peer energy trading in smart grid through blockchain: a double auction-based game theoretic approach. IEEE Access 2021;9:49206–18.

[25] Esmat A, de Vos M, Ghiassi-Farrokhfal Y, Palensky P, Epema D. A novel decentralized platform for peer-to-peer energy trading market with blockchain technology. Appl Energy 2021;282:116123.

[26] Xu J, Paruch K, Cousaert S, Feng Y. Sok: decentralized exchanges (DEX) with automated market maker (AMM) protocols. ACM Comput Surv 2023;55(11):1–50.

[27] Ali L, Azim MI, Peters J, Bhandari V, Menon A, Tiwari V, Green J, Muyeen SM. Blockchain-based local energy market enabling P2P trading: an Australian collated case study on energy users, retailers and utilities. IEEE Access 2022;10:124429–47.
[28] Seven S, Yoldas Y, Soran A, Yalcin Alkan G, Jung J, Ustun TS, Onen A. Energy trading on a peer-to-peer basis between virtual power plants using decentralized finance instruments. Sustainability 2022;14(20):13286.
[29] Lo YC, Medda F. Uniswap and the emergence of the decentralized exchange. J Financ Mark Infrastruct Oct 2020;10(2):1–25. https://doi.org/10.2139/ssrn.3715398.
[30] Bevin KC, Verma A. Decentralized local electricity market model using automated market maker. Appl Energy 2023;334:120689.
[31] Karisma K, Goundar S. Blockchain reshaping energy markets: regulatory frameworks for sustainability-driven energy tokens. In: Goundar S, editor. Cryptocurrencies - innovations, challenges, and future prospects. London:IntechOpen; 2025. https://doi.org/10.5772/intechopen.1013179.
[32] Mohan V. Automated market makers and decentralized exchanges: a DeFi primer. Financ Innov 2022;8(1):20.
[33] Aldrich EM, López Vargas K. Experiments in high-frequency trading: comparing two market institutions. Exp Econ 2020;23(2):322–52.
[34] Ramseyer G, Goyal M, Goel A, Mazières D. Augmenting batch exchanges with constant function market makers. In: Proceedings of the ACM conference on economics and computation (EC '24); 2024.
[35] Mohan V. Automated market makers and decentralized exchanges: a DeFi primer. Financ Innov 2022;8(1):20.
[36] Canidio A, Fritsch R. Batching trades on automated market makers. In: Proceedings of the 5th conference on advances in financial technologies (AFT 2023); 2023. p. 24:1–24:17.
[37] Celig T, Talari S, Ketter W, Schoder D. Automated market maker-based batch auction for decentralized customer-centric local energy sharing. In: 2024 IEEE PES innovative smart grid technologies Europe (ISGT EUROPE). IEEE; 2024. p. 1–6.
[38] Hayes BP, Thakur S, Breslin JG. Co-simulation of electricity distribution networks and peer to peer energy trading platforms. Int J Electr Power Energy Syst 2020;115:105419.
[39] Wang S, Taha AF, Wang J, Kvaternik K, Hahn A. Energy crowdsourcing and peer-to-peer energy trading in blockchain-enabled smart grids. IEEE Trans Syst Man Cybern Syst 2019;49(8):1612–23.
[40] Luo F, Dong ZY, Liang G, Murata J, Xu Z. A distributed electricity trading system in active distribution networks based on multi-agent coalition and blockchain. IEEE Trans Power Syst 2018;34(5):4097–108.
[41] Paudel A, Sampath LPMI, Yang J, Gooi HB. Peer-to-peer energy trading in smart grid considering power losses and network fees. IEEE Trans Smart Grid 2020;11(6):4727–37.
[42] Ullah MH, Park J-D. Network-constrained local energy market clearing for peer-to-peer trading with bilateral power losses. Electr Power Syst Res 2025;245:111600.
[43] Yuan H, Li F, Wei Y, Zhu J. Novel linearized power flow and linearized OPF models for active distribution networks with application in distribution LMP. IEEE Trans Smart Grid 2016;9(1):438–48.
[44] Ullah MH, Park J-D. Peer-to-peer energy trading in transactive markets considering physical network constraints. IEEE Trans Smart Grid 2021;12(4):3390–403.
[45] Tarashandeh N, Karimi A. Peer-to-peer energy trading under distribution network constraints with preserving independent nature of agents. Appl Energy 2024;355:122240.
[46] Zhu J, Liu W, Fang L, Wu R, Chen J. A fully decentralized spatiotemporal decomposition method for real-time peer-to-peer trading in distribution network. Sustain Energy Grids Netw 2025:101729.
[47] Guo Z, Pinson P, Chen S, Yang Q, Yang Z. Online optimization for real-time peer-to-peer electricity market mechanisms. IEEE Trans Smart Grid 2021;12(5):4151–63.
[48] Khorasany M, Mishra Y, Ledwich G. A decentralized bilateral energy trading system for peer-to-peer electricity markets. IEEE Trans Ind Electron 2019;67(6):4646–57.
[49] Lilla S, Orozco C, Borghetti A, Napolitano F, Tossani F. Day-ahead scheduling of a local energy community: an alternating direction method of multipliers approach. IEEE Trans Power Syst 2019;35(2):1132–42.
[50] Zare A, Mehdinejad M, Abedi M. Designing a decentralized peer-to-peer energy market for an active distribution network considering loss and transaction fee allocation, and fairness. Appl Energy 2024;358:122527.
[51] Cui S, Wang Y-W, Shi Y, Xiao J-W. An efficient peer-to-peer energy-sharing framework for numerous community prosumers. IEEE Trans Ind Inform 2019;16(12):7402–12.
[52] Kim HJ, Chung YS, Kim SJ, Kim HT, Jin YG, Yoon YT. Pricing mechanisms for peer-to-peer energy trading: towards an integrated understanding of energy and network service pricing mechanisms. Renew Sustain Energy Rev 2023;183:113435.
[53] Xu L, Wang B. Peer-to-peer electricity trading considering voltage-constrained adjustment and loss allocation in blockchain-enabled distribution network. Int J Electr Power Energy Syst 2023;152:109204.
[54] Zhu C, Byrd RH, Lu P, Nocedal J. Algorithm 778: L-BFGS-B: fortran subroutines for large-scale bound-constrained optimization. ACM Trans Math Softw 1997;23(4):550–60.
[55] Santana C, Albareda L. Blockchain and the emergence of decentralized autonomous organizations (DAOs): an integrative model and research agenda. Technol Forecast Soc Change 2022;182:121806.
[56] Energy Web Foundation. The energy web chain: accelerating the energy transition with an open-source, decentralized blockchain platform, 2019. https://www.energyweb.org/reports/the-energy-web-chain/ [Accessed 20 February 2025].
[57] Vickrey W. Counterspeculation, auctions, and competitive sealed tenders. J Finance 1961;16(1):8–37.
[58] Clarke EH. Multipart pricing of public goods. Public choice 1971:17–33.
[59] Karaca O, Sessa PG, Walton N, Kamgarpour M. Designing coalition-proof reverse auctions over continuous goods. IEEE Trans Autom Control 2019;64(11):4803–10.
[60] Faia R, Goncalves C, Gomes L, Vale Z. Dataset of an energy community with prosumer consumption, photovoltaic generation, battery storage, and electric vehicles. Data Br 2023;48:109218.
[61] Georges Hebrail AB. Individual household electric power consumption. [Dataset]. UCI Mach Learn Repos 2006. https://doi.org/10.24432/C58K54.
[62] SU Eletricidade, 2024. https://sueletricidade.pt/pt-pt/page/601/tarifas-baixa-tensao-normal.
[63] UoC. Ammba market simulation Dec, 2024. https://github.com/INTELLIGENT-UoC/ammba_simulation.
[64] Zhou Y, Wu J, Long C. Evaluation of peer-to-peer energy sharing mechanisms based on a multiagent simulation framework. Appl Energy 2018;222:993–1022.
[65] Palensky P, Dietrich D. Demand side management: demand response, intelligent energy systems, and smart loads. IEEE Trans Ind Inform 2011;7(3):381–8.
[66] Saber H, Ehsan M, Moeini-Aghtaie M, Fotuhi-Firuzabad M, Lehtonen M. Distributed transactive coordination of residential communities aiming at fulfilling households' preferences. IEEE Access 2022;10:122010–21.
[67] Saber H, Ehsan M, Moeini-Aghtaie M, Ranjbar H, Lehtonen M. A user-friendly transactive coordination model for residential prosumers considering voltage unbalance in distribution networks. IEEE Trans Ind Inform 2022;18(9):5748–59.